Wireless Sensing for Material Identification: A Survey

Yande Chen, Chongzhi Xu, Kexin Li, Jia Zhang, *Student Member, IEEE*, Xiuzhen Guo, Meng Jin, Xiaolong Zheng, *Member, IEEE*, and Yuan He, *Senior Member, IEEE*

***Abstract*—As an application of fine-grained wireless sensing, RF-based material identification follows the paradigm of RF computing that fetches the information during RF signal propagation. Specifically, the RF signal accesses the objects' material-related information and carries the information with its electromagnetic properties. With a variety of important applications, research on RF-based material identification has gained significant progress in recent years. However, several fundamental problems remain insufficiently studied, such as the sensing models, signal processing approaches, performance and future extensions. This paper presents the first comprehensive survey of RF-based material identification. According to the basic sensing model used for sensing, we propose a taxonomy to classify the existing works into two categories: reflection-based and penetration-based. The works in each category are further grouped by the type of RF signals used, with elaborated discussion of the detailed approaches and the common challenges. We provide a framework that benchmarks the performance of the existing works, followed by a thorough discussion of future extensions.**

***Index Terms*—Material identification, Wireless sensing, Contactless sensing, Device-free sensing.**

I. Introduction

Wireless sensing has been developing rapidly and has supported applications including object localization and tracking [1], [2], 3D reconstruction [3] and vital sign monitoring [4]. With the availability of fine-grained data such as Wi-Fi channel state information (CSI) [5] and millimeter wave in-phase/quadrature (I/Q) data in recent years, those spatial properties of objects can be measured more precisely. However, the fact that fine-grained data potentially convey more properties of objects (e.g. the material composition) is commonly overlooked.

Research on radiofrequency-based (RF-based) material identification is essential to explore for deeper understanding of the interplay between the material and the signal propagation. Specifically, on the propagation path of communication signals, the media and the reflectors consist of materials that influence the signal according to the penetration and reflection model, respectively. Meanwhile, the parameters of the model depend on their material composition and shape.

Therefore, identifying material composition based on RF signal propagation principles enables novel applications of communication technologies in numerous industrial, research, and civil domains. In the industrial domain, various applications rely on identifying material composition, including product quality control, defect detection and hazardous substance detection. In the research domain, materials from living organisms can be probed in biomedical sciences to detect anomalies [6] and forecast health-related issues [7]. In the civil domain, material identification can be used as a food security tool to determine the expiration status of food products [8], [9] as their chemical compositions change significantly after the expiry period. Similarly, an authentic product can be distinguished from a fake product based on the unique material signature of the original product [10].

Moreover, understanding the impact of materials in communication channels can potentially enhance wireless communication. Inspired by the RF computing paradigm, the RF signal can be regarded as operands that are editable by the in-channel operators (i.e., media and reflectors). On the propagation path of communication signals, the media and reflectors consist of some material that influence the signal according to the penetration and reflection model, respectively. Moreover, the parameters of the model (i.e. dielectric permittivity, thickness) depends on their material composition and shape. For example, a reflective intelligent surface (RIS) can reprogram the signal by elements made of specially designed materials. Typically, each element changes the strength and phase of the reflected/penetrated signal in a dedicated mode and the superposed signal is boosted (e.g. magnified [11] or nullified [12]).

A wide range of RF-based communication technologies are capable of material identification. Furthermore, different features of the technologies bring distinct benefits for material identification. For example, a wide bandwidth (e.g. millimeter wave (mmWave), ultra-wideband (UWB), Terahertz (THz)) can carry more information about the frequency-related response of materials, enabling finer-grained material identification; a shorter wavelength (e.g. mmWave, THz) leads to phase information more sensitive to the effect of material composition, while a longer wavelength (e.g. radio frequency

Manuscript received 24 Oct, 2023; revised 16 Apr, 2024 and 7 Aug, 2024. This work is supported in part by the National Natural Science Foundation of China (No. 62425207, No. U21B2007, No. 62202264, No. 62394344 and No. 61932013) and the Xiaomi Young Talents Program of Xiaomi Foundation.

Y. Chen, J. Zhang and Y. He are with the School of Software, Tsinghua University, Beijing, China (e-mail: cyd22@mails.tsinghua.edu.cn; j-zhang19@mails.tsinghua.edu.cn; heyuan@tsinghua.edu.cn).

C. Xu and X. Zheng are with the School of Computer Science, Beijing University of Posts and Telecommunications, Beijing, China (e-mail: xu-chongzhi@bupt.edu.cn; zhengxiaolong@bupt.edu.cn).

K. Li and M. Jin are with the John Hopcroft Center for Computer Science, Shanghai Jiao Tong University, Shanghai, China (e-mail: likexin0103@sjtu.edu.cn; jinm@sjtu.edu.cn).

X. Guo is with the College of Control Science and Engineering, Zhejiang University, Hangzhou, China (e-mail: guoxz@zju.edu.cn).

identification (RFID), Wi-Fi, UWB, Bluetooth, long range radio (LoRa), long time evolution (LTE)) bring greater penetrability to probe inner layers of objects; low-cost devices (e.g. RFID, Wi-Fi, Bluetooth, LoRa) are most likely to be widely deployed. To the best of our knowledge, RFID [9], [10], [13]–[16], mmWave [6], [17]–[21], Wi-Fi [22]–[24], and UWB [25]–[27] signals have been used for RF-based material identification, covering all the features and enabling a more nuanced understanding of the objects in the environment.

Nevertheless, most existing RF-based material identification works are based on design-specific observations, making them hard to migrate and follow. A comprehensive study on RF-based material identification could potentially solve this problem, yet existing literature only covers localization and tracking methodologies [28] or techniques including fingerprinting [28], mobility [29] or spatial context-based [30] localization, multi-object tracking [31], gesture or gait recognition [32], activity recognition [33] and a comprehensive survey of the recognition tasks above [34].

To fill this gap, we conduct a survey of RF-based material identification in this paper. According to electromagnetic theory, the RF signal can either reflect at or penetrate through a piece of material during propagation. Based on that, we proposed a taxonomy that categorizes prior works into the reflection-based or penetration-based branches. Next, we analyze the common challenges for each category and each type of RF signal. Afterward, we benchmark the performance of RF-based material identification and propose research areas for future exploration. The contributions of this paper are as follows:

- We propose a novel, comprehensive taxonomy of RF-based material identification that originates from electromagnetic laws.
- For the reflection-based and penetration-based modes, we introduce feasible RF signal types for material identification, analyze prior works, and summarize common challenges for each type.
- We point out possible extensions of RF-based material identification for future endeavors, including adapting to more real-life cases and optimizing the performance.

The rest of this paper is structured as follows: the main body (Sections 2-5) focuses on RF-based material identification, followed by a discussion on research spaces (Section 6), and a summary of the paper (Section 7). In the main body, Section 2 introduces the scope and taxonomy of this paper after the definition of material identification. Sections 3 and 4 delve into theoretical analysis and existing work on reflection-based and penetration-based material identification methodologies, respectively. Section 5 compares these methodologies based on several performance metrics. Following the main body, Section 6 discusses potential advancements in material identification for the future, and Section 7 summarizes the whole paper.

II. SCOPE AND TAXONOMY

A. RF-based Material Identification in a Nutshell

RF-based material identification is the process of measuring the frequency response of a material and then analyzing its composition based on the frequency response.

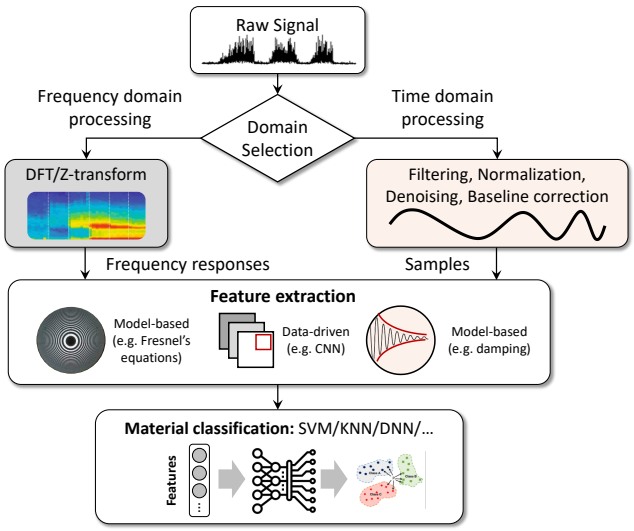

Fig. 1. The typical workflow of RF-based material identification.

To measure the frequency response, the RF signal is emitted, and the reflected signal or the penetrated signal is received. First, with a signal-specific hardware and software toolkit, the amplitude and phase of each time-domain sample in the intermediate frequency (IF) signal or the baseband signal can be obtained. Afterward, frequency-domain or time-domain analysis is applied to the IF or baseband signal. Frequency-domain analysis is applied in most material identification works. The frequency of each component in the signal is typically invariant within the wireless channel, while the amplitude and phase of time-domain samples can be distorted by attenuation and multipath reflection. Moreover, the time-domain dynamics of RF signals is hard to model. Consequently, time-domain analysis can sometimes be applied to near-field signals with data-driven approaches, while frequency-domain analysis is applicable to most scenarios.

In frequency-domain analysis, the signal is first converted to the frequency domain with a DFT operation or a Z-transform operation. After the operation, the received signal strength and phase of each frequency component can be obtained, which is the frequency response. Furthermore, a feature extraction model is built to generate features from the frequency response. It is typically based on physical principles like Fresnel's Equation and Snell's Equation [35], and the features are defined as the dielectric permittivity, the attenuation factor or other properties of materials. Alternatively, data-driven methods like the convolutional neural network (CNN) can be utilized to build an end-to-end feature extraction model.

In time-domain analysis, the features are directly extracted from a series of time-domain samples. The feature extraction model can be either based on physical principles or data-driven.

After time-domain preprocessing and feature extraction, the features are fed into a classification model. For features with explicit physical meanings (e.g. the dielectric permittivity), the model can be as simple as a lookup table that maps

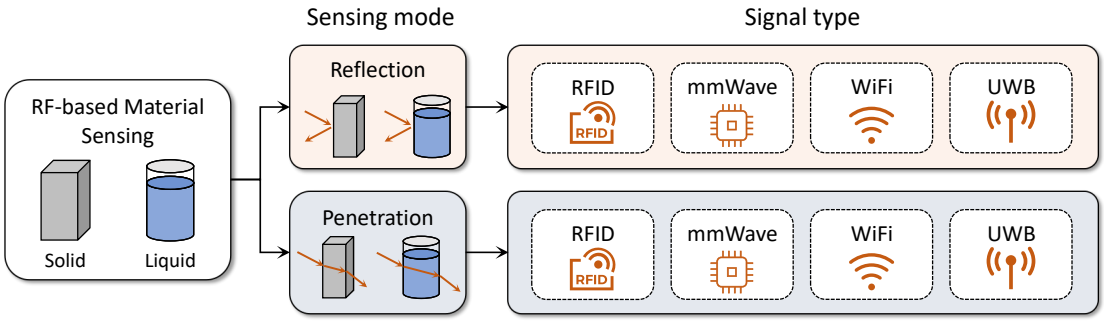

Fig. 2. The taxonomy of RF-based material identification consists of two levels. The first level is sensing mode, including reflection-based and penetration-based material identification. The second level is signal type, which includes RFID, mmWave, Wi-Fi and UWB.

the features to the material composition. For features with implicit connection to the material composition, data-driven approaches like a support vector machine (SVM), a k-nearest neighbor (KNN) model or a deep neural network (DNN) can be applied. These models is typically trained with a pre-collected dataset to estimate the material composition.

The signal propagation process in material identification is similar to that in context recognition [34]. Specifically, the signal typically propagates from the transmitter to the object in free space, reflects at or penetrates through the object (where the material is) and then propagates from the object to the receiver in free space.

Nevertheless, they focus on distinct parts of the propagation process. As spatial information (i.e. range, angle, scale, shape) is crucial for most context recognition tasks like gesture recognition, gait-based identification and vital sign monitoring, the free-space propagation parts, which carry range information, are considered in context recognition. In contrast, they are irrelevant factors in material identification, and the reflection/penetration part during propagation is considered. Therefore, material identification works keep both the object and device static at known positions, or calibrate the absolute position and motion, while context recognition may utilize features related to them (e.g. micro-Doppler features).

B. Taxonomy

As shown in Fig. 2, RF-based material identification methods can be categorized into a two-level structure. The methods are first categorized by their sensing mode (i.e., the utilized signal). Reflection-based material identification relies on the reflected signal, while penetration-based material identification utilizes the penetrated signal or the superposition of both signals. Then, for either of these two categories, different types of signal can be used, which accordingly requires different signal processing techniques to infer the material composition from the signal-type-specific fine-grained data. So we organize the existing works on material identification into a two-level structure, where the first level is classified by the sensing mode (i.e., reflection-based or penetration-based), and the second level provides the classification by the utilized sensing signal.

1) First-level Classification by Sensing Mode: RF signals exhibit different behaviors in the reflection-based and penetration-based modes of sensing. The transmitter and receiver antenna are typically co-located in the reflection-based mode yet distributed on both sides of the object in the penetration mode. Moreover, in the reflection-based mode, the amplitude and phase of the RF signal are relevant to the free-space propagation distance and the material, while the time of flight (ToF) is irrelevant to the material; in the penetration mode, the ToF, amplitude and phase of the RF signal are all relevant to the free-space propagation distance and the material.

The difference further implies different challenges in extracting the material information from the signal. For example, the reflection-based method suffers more from a multipath effect because the environment may contain multiple reflectors; the penetration-based method requires more signal processing techniques because the amplitude and phase of the signal are affected by more factors.

2) Second-level Classification by Signal Type: Material identification methods vary with the type of the utilized signal. The method design corresponds to which signals can be generated under control, how the signal interacts with the material and the environment and what data can be acquired at the receiver.

Various signals exhibit various merits related to their features in material identification. First, the bandwidth positively contributes to the upper limit of material-related information carried by the signal. The material's unique change to the signal is relevant to the frequency of the signal, assuming the signal is single-frequency; for a wideband signal, each frequency component records a different material-related change. Second, the wavelength has a two-sided impact. A longer wavelength fits better for the majority of scenarios, as it enables material identification at a longer range, provides better penetrability to probe the inner layers of the object and tolerates rougher surfaces of the object. Nevertheless, a shorter wavelength implies greater phase sensitivity to the channel variation, enabling finer identification of the penetrated material. Third, the cost of devices has an impact on the ubiquity of material sensing based on each technology.

TABLE I
COMPARISON OF MMWAVE, WI-FI, RFID, AND UWB ON MATERIAL IDENTIFICATION PERFORMANCE.

Signal	Bandwidth	Scale	Range	Cost	Modification	Adaptability
RFID	500 MHz	dm-level	meters	$ 1300	Tag attachment (tag-based)	Multiple objects (tag-based), obstacles
mmWave	4000 MHz	cm-level	meters	$ 900	Not required	Multiple objects, multipath
Wi-Fi	160 MHz	dm-level	meters	$ 24	Hardware/Software modification	Obstacles
UWB	1500 MHz	dm-level	meters	$ 250	Not required	Obstacles

Moreover, to be applied to material identification, a communication technology should support controlled signal generation and raw signal magnitude or phase acquisition. Within the spectrum of RF signals, a wide range of technologies including RFID, mmWave, Wi-Fi, UWB, LoRa [36]–[38] and Bluetooth satisfy the first requirement, while ambient LTE and TV signals are excluded as they carry unwanted and unpredictable information. Within the candidates, the RFID, mmWave, WiFi and UWB technologies provide data in the second prerequisite (i.e. the received signal strength and phase of RFID and UWB, the I/Q samples of mmWave and the CSI of Wi-Fi).

Considering representativeness and feasibility, RFID, mmWave, WiFi and UWB are analyzed in this paper.

They cover all types of merits and provide different benefits in material identification: RFID-based methods provide flexibility in deployment; mmWave-based methods leverage the high space resolution of the mmWave signal to extract extra information from the received signal, such as the object-to-radar distance, angle, and velocity; the ubiquity of Wi-Fi signals supports pervasive material identification applications; UWB-based methods utilize the ultra-wideband of the UWB signal for more information on the relationship between material properties and frequency. A detailed comparison of the technologies is presented in Table I and Sec. V.

In this paper, we will discuss the design principle of different sensing modes with their merits, which leads to the selection of appropriate sensing modes or signals for certain sensing applications and inspires the exploration of new types of sensing methodologies.

III. REFLECTION-BASED METHODOLOGY

A. Reflection Channel Model

In reflection-based material identification, the TX antenna transmits an RF signal S_0 towards the object, which reflects the signal to the RX antenna. In the frequency domain, the signal received at the RX antenna is represented as [39]:

$$S = H_{in} * H_I * H_{out} * S_0 \tag{1}$$

where H_{in} and H_{out} denote the signal's *channel distortion* along the TX-to-object path and the object-to-RX path, respectively; H_I denotes the signal's channel distortion caused by its reflection at the surface of the object.

For most material identification methods, frequency-domain analysis (the left part of Fig. 1) is applied. In the frequency domain, the model can be represented as [40]:

$$S(f) = H_{in}(f)H_I(f)H_{out}(f)S_0(f) \tag{2}$$

where f is the frequency of each frequency component.

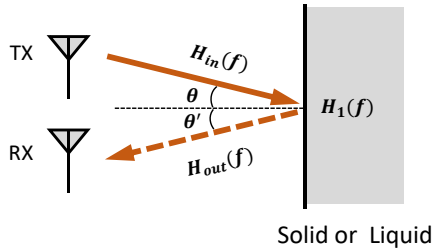

Fig. 3. The reflection model. The reflection model applies to both solid and liquid. The point of reflection is on the surface of the solid or liquid. θ is the angle of incidence. θ' is the angle of reflection. θ is equal to θ'.

TABLE II
PARAMETER SETTINGS AND USAGES IN THE REFLECTION MODEL.

Parameter	Setting	Usage
θ	$\theta = 0°$	single device and static setting
	$\theta \neq 0°$	multiple devices or dynamic setting
$\varepsilon(f)$	$\varepsilon(f) = C$	narrow band, e.g. Wi-Fi, RFID
	$\varepsilon(f) = -kf + b$	wide band, e.g. UWB, mmWave

In this way, the amplitude and phase of the RF signal are affected by the material, as shown in Fig. 3. The effect, which is modeled as the *material-related channel distortion* $H_I(f)$, depends on the both composition and surface roughness of the material. The former determines the reflection coefficient of the material [35], while the latter determines the law of reflection that the signal follows, i.e., whether the reflected signal follows the *specular reflection* model or the *diffuse reflection* model [41].

1) Specular Reflection: Specular reflection changes the propagation direction, amplitude and phase of a RF signal when it makes contact with a flat surface.

As shown in Fig. 3, the reflected signal travels in a direction symmetric to the incident signal against the normal line (i.e., the line perpendicular to the material surface). That is to say, we have the incident angle θ equal to the reflection angle θ'.

In practice, the incident angle is chosen according to the setting. In the case where only one device is used in the sensing application, the incident angle should typically be set at $\theta = 0°$ to make sure that the reflected signal can be captured by the RX antenna of the sensing device. In the cases where multiple devices are used or the object is moving, θ is typically non-zero.

The phase and amplitude change of the reflected signal is

determined by Fresnel's Law [35]:

$$H_I(f) = \frac{\sqrt{\varepsilon(f)}\cos\theta - \sqrt{1-(\sin^2\theta)/\varepsilon(f)}}{\sqrt{\varepsilon(f)}\cos\theta + \sqrt{1-(\sin^2\theta)/\varepsilon(f)}} \quad (3)$$

where $\varepsilon(f)$ denotes the *complex dielectric permittivity* of the material. As a unique property of materials, the complex dielectric permittivity can be utilized to identify them. Moreover, it varies with the frequency of the incident signal, and the variation can be modeled by the Cole-Cole model [42].

The complex dielectric permittivity-frequency curve can be an important indicator of materials. In practice, a linear approximation of the curve is commonly applied, as shown in Tab. II. If a narrow-band signal is used, the dielectric permittivity can be considered as a constant value C. In contrast, if a wide-band signal is used, the dielectric permittivity $\varepsilon(f)$ should be considered as a function of the signal frequency f. Specifically, since the bandwidth of a typical RF signal is typically not higher than 4 GHz, the change in $\varepsilon(f)$ of common materials within the bandwidth can be approximately considered as a linear function of f [43], [44].

2) Diffuse Reflection: Leveraging the diffuse reflected signals is hard because the signals are weak. If the surface is rough, i.e., its surface roughness [45] approaches or exceeds the signal wavelength, the signal will not follow the rules of specular reflection. Instead, the incident signal will be scattered at many angles rather than at just one angle as in the case of specular reflection. Although the distribution of received signal strength (RSS) over different reflection angles is difficult to predict, it is clear that the received signal in diffuse reflection mode is much lower than that in the specular reflection [22].

B. Reflection-based material identification Designs

Reflection-based material identification designs share two challenges:

- **Sensing signal extraction**. Besides the signal reflected from the object, the RX antenna also receives interference from multipath reflections. So, we need a method to extract the object-reflected signal from the superposed signal.
- **Reflection effect modeling.** The relationship between the material of the object and the features of the reflected signal is not clear. We need a clear and reliable model to capture such a relationship.

The solution to the above challenges varies across different signal types. In the rest of this section, we provide solutions to these challenges when using different types of sensing signals.

1) RFID: The usage of RFID tags in material identification can be highly flexible, including applying them to rough or tilted surfaces. This feature comes from the unique mechanism of RFID reflection. Unlike the common reflection-based material identification model, the material composition affects the reflected signal through capacitive coupling [46]. Specifically, when a tag is attached to an object, the coupling effect between the tag's antenna and the material affects the impedance of the tag [13] and further the strength of the reflected signal [47]–[51]. The extent of the change is determined by the dielectric permittivity ε of the material [52]. The reader can then use this feature to identify the object's material. Based on this principle, numerous studies [9], [10], [13]–[15], [53]–[55] have been conducted to identify materials with RFID technology.

Nevertheless, sticking RFID tags may bring unacceptable deployment overhead in some scenarios. To solve this issue, the reflection-based material identification model can be applied. Specifically, the reader and the tag are fixed, and the reader-object-tag path is utilized for sensing.

The first in the line of RFID-based material identification studies is **RFIQ** [9]. It was designed to identify the properties of a container's contents without physically opening it or coming into contact with its contents. This enables non-invasive sensing of food quality and safety. RFIQ's underlying principle is given as follows: an RFID antenna on a filled container as shown in Fig. 4 can reduce the antenna's efficiency and alter its optimal operation frequency, as the antenna design does not account for the new substrate material. Specifically, a filled container couples with nearby RFID tags and alters the signal strength and phase at each frequency point. Therefore, the optimal operation frequency (a.k.a. tuning frequency) changes according to new signal strength values. To capture the new tuning frequency as the characteristic of the contents, RFIQ uses a two-frequency excitation technique to sense changes in the tag's response over a wide bandwidth. By sweeping over a range of sensing frequencies and using a classifier to extract the most salient features, RFIQ can discover the new tuning frequency. Experimental results demonstrate that RFIQ can classify between different mixtures with an average accuracy of 97% [9].

One problem of RFIQ is that the measured tuning frequency is sensitive to environmental factors like tag-reader distance and multipath, thus it suffers poor environmental generalization and only supports coarse-grained material identification. To solve this problem, **Tagtag** [13] proposes to use the tag's phase shift measured under different frequencies as a unique pattern for material identification. This design is based on the fact that the impedance of a tag's antenna changes when it is close or attached to an object, which further leads to a change in the tag's phase shift and the amount of change is related to the object's material type. Therefore, the impedance-related phase change can be used as a metric for material identification. To further remove the tag-reader distance dependency, Tagtag measures the phase shift of the tag at two different locations and combines the measurement results to cancel out the distance-related phase shift. Then a Dynamic Time Warping (DTW) algorithm is used to process the material pattern of the tags and identify the material type accurately. Experimental results demonstrate that Tagtag achieves an average identification accuracy of 93.7% for 7 solid materials and 95.1% for 16 liquids, with an average accuracy of 95.3% for similar liquids [13].

One common problem of the prior proposals is that they require strict measurement conditions. Specifically, in the measurement process, they either require users to extract liquid samples and place them in specialized containers (which often

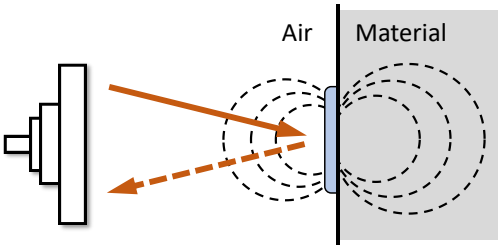

Fig. 4. The principle of RFIQ. RFID tags are coupled with the material that alters the strength and phase of the incident signal.

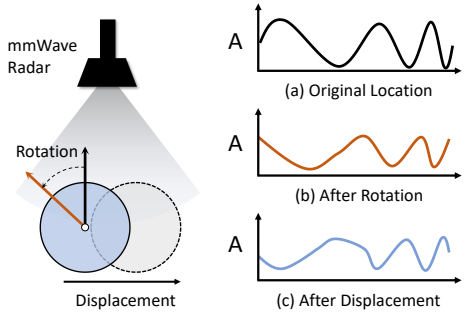

Fig. 5. Illustration of FG-Liquid.The transmit signal of mmWave radar is constant. (a), (b) and (c) are the signals of the container in the original position, the signal after the container rotation, and the signal after the container displacement, respectively.

involves a complex calibration process), or they can only operate correctly in a single lab setup. This is because the reflected signal is not only impacted by the liquid inside the container but also by the container and the environment where the measurement is made. Besides, most prior proposals can hardly extend to new objects (i.e., unseen material or liquid). In this condition, **RF-EATS** [10] is proposed to improve the generalization of RFID-based material identification, making it immune to environmental variations and can generalize well to unseen environments. The core of RF-EATS is a neural learning model that can effectively learn signal features that are solely attributed to a container's content while ignoring the ones resulting from environmental factors. However, training such a model usually requires a very large dataset, which is especially challenging in the wireless sensing context due to the limited availability of RF datasets. To solve this problem, RF-EATS further proposes an autoencoder to generate a vast amount of realistic multipath-affected data. To enhance the efficiency of extending a model to new contents, RF-EATS employs a transfer learning model, which divides a multi-layered network into common layers and task-specific layers. When learning a new task, RF-EATS can inherit the common layers from a well-trained model and focus on fine-tuning task-specific layers. This largely reduces the training cost. RF-EATS was evaluated in 20 different environments with different measurement conditions. Experimental results demonstrate that RF-EATS achieves an accuracy of up to 90% [10] in most applications, even when tested in unseen environments. Furthermore, the transfer model employed by RF-EATS allows it to achieve a level of accuracy that is close to optimal, even when trained on as few as 4 data samples [10].

Sensing one object can involve multiple RFID tags. In recent years, intelligent reflective surfaces (IRS) [56], [57] have witnessed rapid development, and the one-tag-one-reader (1T1R) structure is revisited. By combining multiple RFIDs into a tag array, Lv et al. [14] leverage the weak coupling between RFIDs and their immediate surroundings to analyze how the signals from the tags correlate with the characteristics of the objects being tagged. While the resonant frequency of UHF RFID tags varies among various objects, such information alone is insufficient to differentiate between materials with high accuracy, as the weak coupling is limited. Thus, this work focuses on analyzing the mutual coupling between tags in an array. In a tag array, the mutual coupling is mainly influenced by material properties, and any quality changes in the material are manifested in the signals simultaneously emitted by the tags in the array. Experimental results demonstrate that the input impedance of the antennas is more complex in the RFID tag array than a single tag,providing more useful information in examining tagged material quality.

Also powered by RFID tag arrays, **RF-ray** [15] is a non-invasive system that enables the simultaneous recognition of an object's shape and material. Unlike other methods that require tags to be attached to the object, the RF-ray system utilizes an array of 7x7 RFID tags and places the object in proximity to it. Therefore, the RFID signals are affected not only by the object's shape, primarily through propagation effects, but also by its material, primarily through coupling effects. RF-ray utilizes a sensing capability enhancement module, along with a two-branch neural network, to analyze the signals generated by its tag array for shape profiling and material identification. To further enhance the system's ability to recognize unseen materials, the authors have incorporated a zero-shot embedding module that utilizes linguistic features. The performance of the system was evaluated on 7 solid objects and 14 liquids. Experimental results demonstrate that RF-ray achieves high accuracy rates for material identification (99.9% [15]). Moreover, the system accurately predicted unseen materials, with an accuracy rate of above 92.9% [15].

Except for the coupling-based methodology above, the classical reflection model is also applied to RFID-based material identification in emerging works [58], [59] to realize device-free material identification and enable handheld material identification devices. Instead of being attached to the material or container, the tag is statically placed relative to the reader. Emitted from the reader, the RFID signal is reflected at the material surface, backscattered by the tag, and then reflected again at the material surface towards the reader.

However, leveraging the link with the three reflections above is challenging because the line-of-sight (LOS) path between the reader and the tag introduces severe interference. Existing works [58], [59] simply yet effectively solve the problem by

blocking the LOS path. For instance, **Tamera** [58] simultaneously tracks and recognizes the object with two independent groups of reader and tag array. Each group estimates an AoA of the object with the phase of received signals at each tag. Therefore, the object can be localized, and the movement of objects can be detected. When the object moves, the amplitude and phase of the reflected signal change, and the ratio of the amplitude change to the phase change indicates the reflectivity and the material composition of the object.

2) mmWave: mmWave-based sensing has an advantage in precision [60]–[63] and ubiquity [64]–[68]. However, some of such works require a specified experimental setup and the system could be more expensive than systems operating at lower frequencies. It's also challenging to find features related to the material instead of the environment.

The foremost origin of precision is the mm-level wavelength and GHz-level large bandwidth. Such properties enable precise detection of objects. Besides, the majority of mmWave-based material identification relies on the frequency-modulated continuous wave (FMCW). The critical advantage of FMCW is its ability to separate reflections of multiple reflectors and focus on the object. By comparing the transmitted and received FMCWs, information about the range, velocity, and angle of the objects can be available [69]. With the three indicators above, the reflectors are projected into a three-dimensional space, and the object is unlikely to collide with other reflectors. Moreover, mmWave radar provides precise strength and phase measurements of received signals. The strength can classify materials by reflection coefficients [70]–[72], while the phase is a fine-grained indicator of the distance [21], [73].

On the other hand, the compact and lightweight nature of mmWave radar makes it a more feasible option for widespread implementation in comparison to bulky RFID readers. Moreover, contrasted with RFID-based sensing, mmWave-based material identification is device-free at the material side, as the mmWave signal directly reflects on the material surface.

As a pioneering work, **RadarCat** [17] explores the outstanding information capacity of mmWave to classify a large set of materials and objects, paving the way for new possibilities for seamless interaction with digital devices in everyday contexts. RadarCat is based on time-domain analysis of near-field mmWave reflected signal. The system capitalizes on the multi-channel FMCW radar signals emitted by a Project Soli sensor, which exhibit distinct characteristics of different objects depending on their material, thickness, and geometry when the signal is bounced off. The signals themselves are quite distinctive due to the informative near-field propagation and 4 GHz bandwidth, and by applying machine learning to them, RadarCat can accurately extract information about the material composition of the object, enabling a range of innovative interaction capabilities. Experimental results demonstrate that the system achieves classification accuracy of 99.97% when categorizing 26 different materials [17].

Replacing near-field reflection with the far-field one introduces an analytical model of signal and yields model-driven methods. For example, **mSense** [18] quantitatively characterize the material's reflection coefficient for mobile material identification. Guided by the observation that various objects reflect incident electromagnetic waves to different degrees depending on their constituent materials, mSense introduces a novel material reflection feature (MRF) that provides a quantitative characterization of a material's reflectivity, which is unaffected by environmental factors. With the sanitized Channel Impulse Response (CIR), mSense calculates the MRF to identify the material type by selecting the best-matched record. Experimental results demonstrate that the system is capable of categorizing five commonly occurring material types with an average accuracy of 93% [18], regardless of their respective sizes and thicknesses.

Models can be combined with data-driven methods. **FG-LiquID** [19] aims at fine-grained and robust classification of materials. This innovative method utilizes a dataset of non-material factors to suppress their impact on the material measurement. Such a dataset is more convenient to collect with FMCW mmWave signal than others because FMCW carries the most common non-material factors including range, angle, and velocity information. As shown in Fig. 5, FG-LiquID utilizes a 60 GHz mmWave Radar equipped with a 2×4 antenna array to collect the RSS, rotation, and displacement over 100 different settings. With RSS as reflection (R) input and the rest data as calibration (C) input, FG-LiquID incorporates an elaborate neural network called RC-Net to automatically remove interference and generate material-dependent features. Experimental results demonstrate that FG-LiquID can effectively differentiate among 30 distinct types of liquids, achieving an average accuracy rate of 97% across five distinct scenarios [19]. Moreover, the system is capable of discriminating very similar liquids, such as liquors with only a 1% difference in alcohol concentration by volume.

The mmWave-based model can also be combined with vibrometry. With a 77-GHz mmWave radar, RFVibe [74] classify materials by mechanical features after the material is stimulated by an audio sound. Specifically, the amplitude of vibration is related to the frequency of the audio sound, and the maximum amplitude as well as its corresponding frequency are indicators of the material. Moreover, the duration of vibration after the audio sound stops can also be an indicator named the damping feature. Combining the three indicators yields a 81.3% classification accuracy of 23 objects made of 7 distinct materials.

The state-of-the-art material identification precision is achieved by a mmWave-based combined method. By carefully designing the sensing device and signal processing techniques, Liu et al. [6] have developed an FMCW-based method for measuring **glucose** concentration that resolves up to 0.1 mg/mL for ex vivo glucose measurements using a 77-GHz FMCW radar. To ensure accuracy, the authors utilized a 3D printed device to secure the position of the radar and container and a microwave-absorbing sponge to minimize external interference. The container was paired with an injector for solution replacement to eliminate any effects caused by surface mismatch and to ensure consistent monitoring of the same volume of solution. The system relies on the fact that variations in the dielectric constant of glucose produce corresponding changes in the amplitude and phase of the radar echo signal. Therefore, the amplitude and phase of the radar echo signal can be used

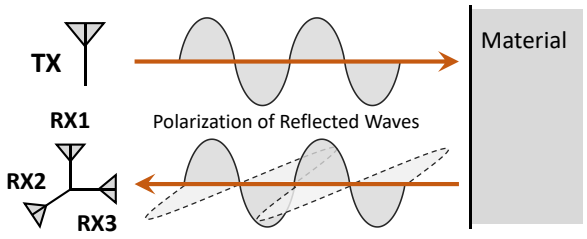

Fig. 6. Illustration of IntuWition. With three orthogonally polarized receiving antennas, the polarization of the reflected wave can be measured and translated to the textures and materials of the objects.

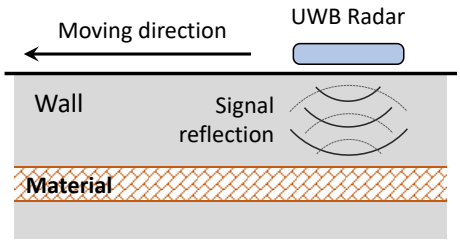

Fig. 7. The overview of SiWa. SiWa uses the penetration of UWB signals to identify object materials within the wall and moves the UWB radar to image the objects.

to differentiate solutions of varying glucose concentrations. However, glucose concentration cannot be determined with a single fitting curve. To address this, they employed a method that combines Continuous Wavelet Transform (CWT) and Neural Network to explore the correlation between glucose concentration and the radar echo signal. Similarly, **AgriTera** [8] leverages a broadband sub-THz signal (100-400 GHz) to measure the fruit ripeness indicators Brix and Dry Matter with a relative mean squared error of 0.55%. After collecting a dataset containing the reflectivity at each frequency in the spectrum and the real Brix and Dry Matter values, AgriTera trains a Partial Least Square Regression (PLSR) model which is leveraged to predict the Brix and Dry Matter of apples, persimmons and avacados.

3) Wi-Fi: Wi-Fi can be an outstanding choice for indoor and cost-sensitive scenarios [75]–[77]. Compared to mmWave technology, which is susceptible to signal blockage by walls due to its short wavelength, Wi-Fi signals have the advantage of being able to penetrate walls and occlusions [78], making them a more competitive option for detecting occluded objects. Furthermore, Wi-Fi technology is relatively inexpensive, lightweight, and already integrated into many mobile platforms. As a result, there has been a growing interest among researchers in leveraging commodity Wi-Fi for sensing purposes [79]–[83].

In the realm of material identification, the reflected Wi-Fi signals can be utilized. It is feasible to place one Wi-Fi transceiver facing the object, or place a transmitter and a receiver on the same side of the object. Nevertheless, the strong penetration ability of Wi-Fi signals makes it difficult to use them for material identification based on reflection. Wi-Fi signals can easily penetrate common objects, resulting in a reflected signal from the inner surface of the object and superimposing with the outer signal. This superposition requires a complex extension of the reflection model in Sec. III, which impedes the development of related material identification.

Fortunately, another signal property called polarization can solve the problem. Wi-Fi signals are naturally linearly polarized (i.e. have a specific polarization angle), and reflection changes the polarization angle or makes the signal unpolarized according to the reflector's material composition. Furthermore, the superposition challenge can be tackled with the principle that two polarized signals combine into a polarized signal, and an unpolarized signal yields an unpolarized superposition with any signal in most cases. As a validation of the principles above, **IntuWition** [22] enables the sensing of the location and material properties of objects, even when they are occluded. At its core, IntuWition infers material properties by measuring the wireless signals that reflect off objects, specifically by capturing the polarization of the reflected waves. Because of the texture and material differences among objects, distinct polarization changes are observed in the reflected waves after reflection off the surfaces of different objects. By measuring the polarization of reflected waves from surrounding objects, one can infer their material composition. IntuWition is inspired by radar polarimetry [84] and employs a vertically-polarized transmitter antenna and three mutually-perpendicular polarized receiving antennas to measure the Wi-Fi signal, as shown in Fig. 6. The measured power is then used to infer the material composition via a multi-layer perceptron model [85]. Additionally, the system can accurately locate surrounding objects by measuring the time of flight along different paths. Experimental results demonstrate that the system can distinguish between 5 types of materials of various sizes and orientations with high accuracy rates. Specifically, the system achieves an accuracy rate of 95% in line-of-sight scenarios and 92% in non-line-of-sight settings [22].

The polarization-based principle can be integrated with classical CSI-based techniques. Shi et al. [23] have developed an object identification system for in-baggage items that can be easily deployed in various environments. The system utilizes Wi-Fi signals bouncing off an object's surface, with the polarization of the reflected signals providing valuable information about the material of the object. As a result, analyzing the polarization of reflected Wi-Fi signals enables the system to distinguish objects made of different materials. Specifically, the system uses calibrated CSI measurements to extract two sets of features: polarization features and CSI complex difference statistics. Based on these features, a deep learning model is developed for object identification. Furthermore, the system incorporates a material-based domain adaptation technique that employs adversarial learning to facilitate rapid deployment in diverse environments. Experimental results demonstrate that the system can achieve object identification accuracy exceeding 97% [23] when operating within the same environment. Moreover, when the system is deployed in a new environment with minimal training, the domain adaptation technique can improve object identification accuracy by as much as 42% [23].

4) UWB: Ultra-Wideband (UWB) technology, which has been widely used in various sensing applications [86]–[89], can also be an effective choice. It is capable of transmitting signals across a broad bandwidth. Based on their response to signals with significantly different frequencies, UWB signals can be utilized in material identification [25], [26]. In UWB signals, the frequencies are transmitted simultaneously, resulting in quicker sensing than mmWave. However, this comes at the cost of reduced ability to filter interfering objects in the range, velocity, and angle dimensions.

Besides, the UWB signal has strong penetration capabilities and supports in-wall material identification. A typical setup of reflection-based UWB sensing is to place a UWB transmitter and a receiver at the same side of a buried object. **SiWa** [25] is an affordable and portable system designed for wall inspections that can create a synthesized image of a wall's structure and identify its material status. This capability is achieved by simply swiping the SiWa probe along the wall surface without requiring repetitive parameter tuning or calibration, as shown in Fig. 7. The system's hardware front-end, which comprises an IR-UWB chip and antennas, acquires a Synthetic Aperture Radar (SAR) data matrix composed of two-channel polarized and wideband signals. Subsequently, this SAR data matrix is input into the Imaging Network (I-Net) to generate a structural image. The output of the I-Net serves as a guide for further processing of one-dimensional signal samples through the Material Identification Network (M-Net) to identify and diagnose the material. To assess SiWa's ability to identify materials, its performance was evaluated on different in-wall structures. Experimental results demonstrate that SiWa achieves an overall accuracy of 95.2% [25] for identifying the material.

5) Summary: The reflection-based methodologies cover a broad range of scenarios. These methodologies can be a suitable choice for material identification in most cases, and the signal type can meet various requirements: RFID supports flexible solutions and can be the default choice; mmWave helps to achieve high sensing precision; Wi-Fi and UWB are recommended if the object is not exposed to air.

IV. PENETRATION-BASED METHODOLOGY

A. Penetration Channel Model

In reflection-based material identification, the TX antenna transmits an RF signal S_0 towards the object, wherein the signal propagates towards the RX antenna. For most material identification methods, frequency-domain analysis is applied. In the frequency domain, the signal received at the RX antenna is represented as:

$$S(f) = H_{in}(f)H_I(f)H_{out}(f)S_0(f) \tag{4}$$

where $H_{in}(f)$ and $H_{out}(f)$ denote the signal's *channel distortion* along the TX-to-object path and the object-to-RX path, respectively, which is a function of the signal's frequency f. $H_I(f)$ denotes the signal's channel distortion caused by its interaction with the surface and interior of the object during the penetration process.

The material-related channel distortion $H_I(f)$ belongs to one of the three cases below determined by the diameter and roughness of the material surface. Specifically, if the diameter of the material surface is significantly longer than the wavelength of the RF signal, *spectral refraction* [35] or *diffuse refraction* will take place according to the surface roughness [41]. Otherwise, *refraction-diffraction* [90] will take place where the diffraction signal travels *around* the object and sums up to the refracted signal.

1) Penetration with Spectral Refraction: Penetration with spectral refraction is widely used in material identification as it has the simplest model among the three penetration modes. As shown in Fig. 8, an RF signal penetrates a piece of material in three steps: *refraction in*, *propagation inside*, and *refraction out*.

Refraction at Material-Air Interfaces. Refraction changes the direction, amplitude, and phase of the incident signal.

The refracted signal travels along a direction other than the incident one [35]:

$$\theta''(f) = \arcsin \frac{\sin\theta}{\sqrt{|\varepsilon(f)|}} \tag{5}$$

where θ'' represents the angle between the normal line and the refracted signal.

The amplitude and phase of an incident signal are also changed after refraction, namely the refraction-related channel distortions $H_{I,in}(f)$ and $H_{I,out}(f)$. A refracted signal is always paired with a reflected signal, and the electromagnetic boundary condition [91] implies:

$$1 + H_{I,in}(f) = \sqrt{\varepsilon(f)}H^r_{I,in}(f) \tag{6a}$$

$$1 + H_{I,out}(f) = \sqrt{\varepsilon(f)}H^r_{I,out}(f) \tag{6b}$$

where $H^r_{I,in}(f)$ and $H^r_{I,out}(f)$ denote the material-related channel distortion $H_I(f)$ in the reflection model in Sec. III-A1.

Propagation Inside. The material composition determines the time of flight (ToF) and attenuation during propagation within the object. The speed of a RF signal is dependent on the medium's material composition. In vacuum or air, a RF signal travels at a speed of $c_0 = 3 \times 10^8 m/s$; in another medium with a dielectric permittivity of $\varepsilon(f)$, the speed is

$$c = \frac{c_0}{\sqrt{\varepsilon(f)}} \tag{7}$$

Therefore, through a layer of material with thickness d, the ToF is

$$t = \frac{d}{c} = \frac{d\sqrt{\varepsilon(f)}}{c_0} \tag{8}$$

and the phase shift is

$$\Delta\varphi = 2\pi f t = \frac{2\pi f d\sqrt{\varepsilon(f)}}{c_0} \tag{9}$$

Besides, the attenuation of the signal during propagation within the object can be represented as [26]:

$$\frac{A}{A_0} = e^{-\beta d} \tag{10}$$

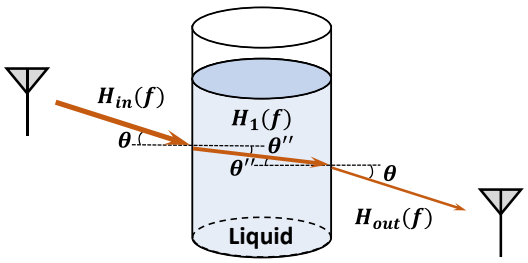

Fig. 8. The penetration model. Take liquid as an example of the object: the signal is refracted at the interfaces between the liquid and the container. θ is the angle of incidence. $\theta^{''}$ is the angle of refraction. The effects of the container on the signal can be neglected because of its low thickness.

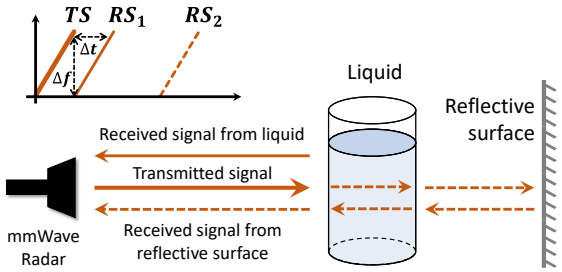

Fig. 9. The overview of mmLiquid. The transmitted signal is received in two paths. One is the signal reflected by liquid. The other is the signal penetrates the liquid and is reflected by the reflective surface. TS is the transmitted signal. RS_1 is the received signal from the liquid. RS_2 is the received signal from the reflective surface.

TABLE III
LIST OF NOTATIONS IN THE PENETRATION-BASED MODEL. THE FIRST THREE LINES ALSO APPLY TO THE REFLECTION-BASED MODEL.

Notation	Meaning
f	Signal frequency
$S(f), S_0(f)$	Strength and phase of received signal and transmitted signal at frequency f
$H_{in}(f), H_{out}(f)$	Channel distortion from the transmitter to the material, and from the material to the receiver
$H_I(f)$	Material-related channel distortion
$H_{I,in}(f), H_{I,out}(f)$	Refraction-related channel distortion when entering and leaving the material
$H_{I,pro}(f)$	In-material channel distortion

TABLE IV
PARAMETER SETTINGS AND USAGES IN THE PENETRATION MODEL.

Parameter	Setting	Usage
θ	$\theta = 0°$	static setting
	$\theta \neq 0°$	dynamic setting
d	fixed	for fine-grained measurement
	variable	for ubiquitous sensing
$\varepsilon(f)$	$\varepsilon(f) = C$	narrow band: Wi-Fi, RFID
	$\varepsilon(f) = -kf + b$	wide band: UWB, mmWave

where β is the attenuation factor and d is the distance of propagation. This equation shows that a RF signal attenuates exponentially in liquid or solid mediums [92], which is different from the inverse square attenuation in free space [93].

Summing up the components above, the channel distortion $H_{I,pro}(f)$ within the object can be represented as

$$H_{I,pro}(f) = \frac{A}{A_0} e^{\Delta\varphi} = e^{-\beta d + j\frac{2\pi f d\sqrt{\varepsilon(f)}}{c_0}} \tag{11}$$

Putting Things Together. According to the three steps in Sec. IV-A, the material-related channel distortion for the frequency f is

$$H_I(f) = H_{I,in}(f) H_{I,pro}(f) H_{I,out}(f) \tag{12}$$

Furthermore, unfolding the entire penetration channel model yields:

$$S(f) = H_{in}(f) H_{I,in}(f) H_{I,pro}(f) H_{I,out}(f) H_{out}(f) S_0(f) \tag{13}$$

This matches the five steps involved in signal propagation through the air and material.

Parameter Settings. Different settings of parameters fit different scenarios as shown in Tab. IV. As in the reflection model, the incident angle θ depends on settings and the model of dielectric permittivity relies on signal bandwidth. Additionally, whether the material thickness d is fixed depends on the application purpose. If the objects are arbitrary, it will be unrealistic to fix their thickness d. In cases where precision is a dominant metric, rather than ubiquity, it may be effective to set d to a fixed value by applying a certain container. Alternatively, the thickness d can be determined by fixing one side of the object and localizing the other side with existing precise localization techniques [94]–[98].

2) Penetration with Diffuse Refraction: Diffuse refraction typically produces extremely weak and unpredictable penetrated signals that are hard to use. As a side product of diffuse reflection occurring at rough surfaces, the diffuse refraction signal is also scattered and unpredictably oriented. After propagation inside the material, the scattered signals reach the other surface of the material with unpredictable incident angles, thus producing scattered and unpredictable penetrated signals. No research works have implemented material identification based on this penetration mode to the best of our knowledge.

3) Penetration with Refraction-Diffraction: The penetrated signal via refraction-diffraction is probably not the best choice for penetration-based material identification, as refraction-diffraction is harder to model yet conveys no extra information about the material composition. When the diameter of the material surface is shorter than or approximately equal to the wavelength of the signal, a portion of the signal will diffract across the material while another portion refracts into the material [90]. On the other side of the material, the diffraction signal and the refraction signal superpose, resulting in the penetrated signal. The strength of the diffraction signal is relative to the ratio between the distance from the material's edge to the TX-RX line and the wavelength (i.e. Fresnel clearance [99]). Compared to the penetrated signal via spectral refraction, the signal implies more about the scale of the material yet nothing more about the composition of the material.

B. Penetration-based Material Identification Designs

The above model associates the material information (i.e. permittivity) with RF signal properties, enabling penetration-based material identification. When it comes to design, two common challenges occur:

- Penetrated signal accessibility: the signal should be able to propagate through the material to the receiver.
- Penetration effect modeling: the relationship between material and modification on signal should be clear, and the modification should be represented as a signal feature.

The solution to those challenges varies among different signal types. Therefore, the rest of this section is grouped by RF signal type.

1) RFID: Instead of attaching tags on materials or containers, tags are regarded as detached transceivers in penetration-based designs [16], [100]. In such designs, the RFID signal travels around between the reader and the tag, penetrating the material. Therefore, the signal properties (e.g. strength, phase, ToF) indicate both the composition and the scale of the material, while reflection-based designs can only sense material composition. However, it is challenging to identify the material composition and object size at the same time.

For instance, **TagScan** [16] can simultaneously image horizontal sections of an object and identify its material composition with an Impinj RFID reader and two linear tag arrays. As shown in Fig. 10, the reader moves along a given trajectory. The basic idea underlying TagScan is that when RF signals penetrate an object, variations in the received signal strength (RSS) and phase are induced by the object's size and material composition. TagScan suppresses multipath signals by weighting the signals received from different tags and different channels. TagScan characterizes each material type with a unique characteristic called the ratio of RSS change and phase change (RP-rate), which is independent of object size. Moreover, the material composition and size can be obtained concurrently using either RSS or phase variation. Finally, TagScan searches for the starting point of all propagation distances and combines all propagation distances to construct the image. Experimental results demonstrate that TagScan achieves a material recognition accuracy of over 94% for 10 different liquids and can distinguish between highly similar liquids such as Coca-Cola and Pepsi [16]. Furthermore, TagScan can generate horizontal cross-sectional images of multiple objects located behind a wall.

2) mmWave: The penetration model introduces more information that helps to adapt to complex scenarios, yet applying the model to mmWave-based designs requires deployment modification.

To leverage the penetration model, it is straightforward to place the object between two radars. However, implementing such designs is challenging due to the difficulty in synchronizing the two radars. Alternatively, the reflective nature of metals can be leveraged to create an equivalent sensing system using a single radar and a metal plane [21]. Specifically, a radar on one side of a metal plane can act as two symmetric radars on two sides. Furthermore, by covering the backside of the material with a metal layer, a radar at the front side can perform penetration-equivalent material identification.

For example, to address the interference of container movement on liquid recognition, **mmLiquid** [20] uses a container position information filtering (CPIF) scheme to eliminate the impact of container location. The system then utilizes a deep complex model (DCN) to classify the liquid. As shown in Fig. 9, mmLiquid uses two steel plates as reflective surfaces, which are placed behind the container and the mmWave radar, respectively. By reflecting some of the mmWave signals off the container and others off the reflective surface, the system can obtain more information about the liquid.

3) Wi-Fi: The penetration model fits Wi-Fi signals well as Wi-Fi has strong penetration ability. The objects on the line-of-sight (LOS) path between the TX and RX antennas have an impact on the Wi-Fi CSI [101], [102]. Therefore, the CSI implies the material on the LOS path, yielding a typical setting involving a transmitter and a receiver with the object in between. However, the low bandwidth and the noise caused by hardware and multipath make it difficult to extract effective material information from Wi-Fi signals.

Drawing the LOS path through a liquid container, **WiMi** [24] implements contactless material identification using ubiquitous and low-cost commercial off-the-shelf (COTS) Wi-Fi devices. Based on the observation that the signal is highly correlated at different frequencies while the noise is not, WiMi removes the impulse noise and reconstructs the useful signal by integrating the correlated signal. For other signal noise that may still be present, the system uses a second antenna to obtain a more stable amplitude ratio than the amplitude readings of a single antenna. To identify materials of different sizes, WiMi uses a material feature that is only related to the material type and not to the object size. This feature contains only the phase difference and amplitude ratio and applies to multi-antenna systems common to 802.11n/ac Wi-Fi access points. Experimental results demonstrate that WiMi can identify 10 common liquids with an overall accuracy higher than 95% [24], even in indoor situations with strong multipath. Additionally, WiMi can distinguish between very similar products such as Pepsi and Coca-Cola.

4) UWB: The interference resistance of UWB signals can be strengthened with the penetration model and proper deployment. In a typical setting, the object is fixed between two antennas that are connected to the same device. Therefore, the multipath effect is likely to be weak, while noise becomes the most significant source of interference. The impact of material penetration on the amplitude and phase of UWB signals is robust to noise because the responses are averaged across all frequencies, and only a few frequencies are affected by noise interference. Therefore, penetration- and UWB-based material identification can be quite robust. It provides the possibility to obtain fine-grained material properties. However, obtaining fine-grained material property needs accurate material-related information. So hardware features that may introduce errors, such as time synchronization and antenna height, should be taken into account.

LiquID [26] uses physics to model the behavior of radio signals inside liquids and estimate the permittivity of liquids to

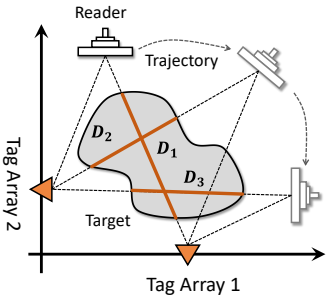

Fig. 10. The system deployment setup of TagScan. The reader moves along the trajectory for imaging. At each position, the reader can make one observation of the object size. D1, D2, and D3 are the observations by the reader at different positions, respectively.

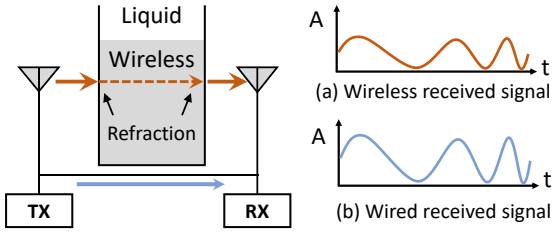

Fig. 11. The system overview of LiquID. The wireless transmission splits between the wire and the wireless antenna. The wired received signal is not attenuated. The amplitude and phase of the wireless received signal are attenuated by the refraction of liquid.

identify them. The basic idea of LiquID is that wireless signals undergo significant slow-down and attenuation as passing through liquids, as manifested by the phase, intensity, and propagation delay of the outgoing signal. As shown in Fig. 11, LiquID connects a wire between the transmitter and receiver, allowing the wireless transmission to be split between the wire and the wireless antenna. By carefully "double-differencing" the wire and air, LiquID measures the relative time of flight (ToF), phase, and RSSI of the liquid with consistent accuracy. To obtain the signal slowdown in liquid, LiquID jointly estimates the phase and ToF. later on, after going through the stages of channel difference, container compensation, and RSSI modeling, LiquID derives an estimate of the permittivity. Experimental results demonstrate that LiquID can calculate the permittivities of 33 different liquids with a median error of 9% [26], which are distributed over the entire spectrum of permittivity. Additionally, LiquID can distinguish between Coke and Diet Coke or Pepsi, whole milk and 2% milk, and other very similar liquids.

UWB-based designs can utilize the relationship of dielectric permittivity and frequency [42] ignored in other works. Inspired by the relationship, UWB-like methodologies are proposed, for example, **LiqRay** [27] analyzes the difference of response at 4 distinct frequencies across 1.7-2.6GHz and enables non-invasive and fine-grained liquid identification without requiring prior knowledge of the container and antenna heights. LiqRay adopts a dual-antenna model based on radio frequency (RF) signals to eliminate the effects of container material and antenna gain. Specifically, LiqRay employs the relative frequency response factor of the liquid material as a feature, which is independent of the container width, as the attenuation factor of the material is related to the signal frequency. Additionally, to eliminate the effect of antenna height, LiqRay models the transmit and receive antennas as thin straight antennas instead of points. When the transmit antenna moves slightly, the electric field below the solution height undergoes a change, which is used to extract the relative frequency response factor. Experimental results demonstrate that LiqRay can accurately identify alcohol solutions in eight distinct solvents with a concentration difference of 1% without prior knowledge, achieving an accuracy rate of 94.92% [27].

5) Summary: The penetration-based methodologies are compatible with scenarios where interference from the environment is a major concern. In different interference-sensitive scenarios, different signal types are recommended: RFID and Wi-Fi are low-cost and easy to deploy; mmWave and UWB can achieve high precision, and mmWave can penetrate small objects.

V. Performance Comparison

This section aims to compare and contrast the performance of material identification models (i.e. reflection and penetration) and signal types (i.e. mmWave, Wi-Fi, RFID, UWB), which primarily links to the gap between material identification research and real-life applications.

A. Metrics

1) Precision and Accuracy: The *precision* of a material identification method refers to the minimal difference between the identification results. It is usually the most important metric because of its strong link to the usability of material identification methods. In this paper, the precision is evaluated with the number of supported types of material.

The *accuracy* of a material identification method refers to the ratio of correct identification results in all results. Since most works claim an accuracy over 90%, it has less impact on usability than precision, and we mainly focus on the precision in the following sections.

2) Device Deployment Overhead: The *device deployment overhead* of a material identification method refers to the cost of the necessary devices, their occupied space and their required modification to run normally.

3) Adaptability: The *adaptability* of a material identification method refers to its usability in complex scenarios. This metric can be evaluated by the maximum range between the device and the object, the resilience to multipath and obstacles and the performance when multiple objects coexist.

B. Comparison of Material Identification Models

1) Precision and Accuracy: If the thickness of the material is known, the penetration model can achieve higher precision than the reflection model; otherwise, the reflection model should be preferred considering the precision.

The precision is boosted by information about *the material composition of the object* yet degraded by that about *unknown*

factors, and both information components rely on the material identification model. In the reflection model, the dielectric permittivity of the material is the only boosting factor, and the distance of signal propagation is the only degrading factor. In the penetration model, the attenuation factor of the material acts as another boosting factor, while the unknown thickness of the object further degrades the precision.

2) Device Deployment Overhead: The cost, space occupation and modification overhead are all heavier for penetration-based methods than reflection-based methods, as the former typically requires two devices clamping the object.

To employ the penetration channel model, it is typical to position the transmitting and receiving antennas on opposite sides of the object [26] to acquire information about the signal as it penetrates the material. This requires a transceiver split device that consists of both transmitting and receiving antennas placed in the same straight line, with the object placed in between them. In this way, the RF signal is emitted from the transmitting antenna, propagates to the surface of the material under test, penetrates inside the object, and ultimately exits from the object to be received by the receiving antenna. Material identification is then achieved by analyzing the difference between the transmitted and received signals. The limitations of the reflection channel model are generally lenient, as there is no need to position devices on both sides of the material, and objects on the ground [103], beside the wall [25], or on human skin [4], [104] are available.

3) Adaptability: The penetration model can support a longer maximum range and better resilience to obstacles, while the reflective model better fits in multi-object scenarios.

Given identical transmission power and receiver sensitivity, the penetrated signal can theoretically be received at a longer range in most scenarios. The same free-space propagation path corresponds to two attenuation terms in the reflection model yet one term in the penetration model, thus the penetration model has an advantage that is hardly diminished by attenuation inside the material.

Besides, the impact of an obstacle on the signal propagation path is non-fatal for the penetration model yet fatal for the reflection model. Another attenuation term in the penetration model can compensate for the impact, while the reflection model is disabled because the reflective surface belongs to the obstacle instead of the object.

Conversely, when simultaneous material identification of multiple objects is required, the reflective model outperforms the penetration model. To meet the requirement of the penetration model that the object lies on the line between two devices, the devices should be moved to different locations for each object, which is infeasible in most scenarios.

C. Comparison of Signals

1) Precision and Accuracy: The difference in bandwidth results in the difference in the precision of material identification. A wider bandwidth implies more information about the material that boosts the precision. The channel distortion equations in both the reflection mode (Eq. 2) and the penetration mode (Eq. 4) are relative to the frequency of frequency components in the RF signal. A wider bandwidth contains more frequency components, generating more equations and a more precise estimation of the dielectric permittivity.

According to Table I, mmWave-based methods can achieve the best precision, followed by UWB, RFID and Wi-Fi.

2) Device Deployment Overhead: The signals have distinct advantages regarding the cost, space occupation and modification overhead.

As a highly pervasive communication technology, Wi-Fi chips cost the lowest, followed by UWB, mmWave and RFID.

Besides, mmWave-based methods require the least space due to minimized transceiver and short minimal distance to the object. The short wavelength of mmWave contributes to both advantages above. The size of the transceiver is limited by the size of the antenna, and the latter is proportional to the wavelength. On the other hand, the minimal distance is required by the far field assumption. As propagation rules in the far field [93] are much simpler than those in the near field [105], most prior works assume that the signal propagates in the far field and requires propagation distances of $\lambda/2$ [106], assuming an antenna size of $D = \lambda/2$. This results in a shorter minimal distance of mmWave than other signals.

Moreover, hardware and/or software modification is required when some signals are applied to material identification. On the material side, some RFID-based works [9], [10], [13] require extra attachments since they depend on RFID tags. Regarding the device side, Wi-Fi-based works may require hardware modification, while mmWave-based ones are the least likely to require such modification. For instance, IntuWition [22] employs orthogonal antennas in the receiver to extract the polarization state of the reflected signal, while a collection of mmWave-based solutions, including RadarCat [17], mSense [18], and FG-LiquID [19], employ different types of mmWave radars, yet no hardware modification is performed.

3) Adaptability: Millimeter-wave-based and some RFID-based methods make it possible to handle scenarios with multiple objects. With well-designed FFT operations that separate signals from different reflectors [107], mmWave-based methods have the best adaptability to multiple-object and multipath-rich scenarios. Besides, with the capability to separate signals through tag-wise activation of RFID tags, RFID-based methods with tags attached to objects are compatible with multiple objects.

Moreover, RFID, Wi-Fi and UWB signals are more resilient to obstacles on the penetration path. According to the Friis Equation [93], the propagation attenuation through an obstacle is proportional to the square of the wavelength.

As the end of the detailed analysis of methodologies for material identification in Sec. III, IV and V, we present Tab. V to recap and summarize prior works.

VI. Lessons Learned

This section discusses shared misconceptions among existing material identification works, as well as common pitfalls for researchers.

TABLE V
PRIOR WORKS ON MATERIAL IDENTIFICATION

Research Work	Model	Features	Frequency (MHz)	Devices	Material	Accuracy
SiWa [25] (2021)	Reflection	Dispersion and polarization	6540-8040	1 movable UWB radar	PVC and rebar	95.2%
RadarCat [17] (2016)	Reflection	Reflection and transmission properties	57000-64000	1 Soli mmWave radar	26 (air, steel, glass, ceramic, porcelain, water, sponge, ...)	96.0%
mSense [18] (2020)	Reflection	Reflection coefficient	58740-61260	2 mmWave radars with 32 antennas each	Wood, plastic, ceramic, water, aluminum	93%
FG-LiquID [19] (2021)	Reflection	Dielectric permittivity	57000-64000	1 mmWave radar	30 liquids (Fanta, Pepsi, Coke, Sprite, milk, 52%/53%/55%/56% alcohol, ...)	97%
RFVibe [74] (2023)	Reflection	Resonant frequency, resonant amplitude and damping feature	77000-81000	1 mmWave radar	Metal, wood, ceramic, glass, plastic, cardboard, foam	81.3%
Glucose [6] (2022)	Reflection	Dielectric permittivity	77000-81000	1 mmWave radar	Human blood (glucose concentration 0.69/0.81/0.91/1.03/1.08 mg/mL)	95%
AgriTera [8] (2023)	Reflection	Reflectivity	100000-400000	1 set of TeraMetrix T-Ray	Avocado, apple, persimmon	0.55% ripeness error
RFIQ [9] (2018)	Reflection	Dielectric permittivity	400-800	1 tag on the container, 1 RFID reader as Tx, 1 USRP N210 as Rx	0%/25%/50%/75%/100% tainted alcohol; 0%/10%/20%/30% adulterated baby formula	96%
Tagtag [13] (2019)	Reflection	Dielectric permittivity	902.75-927.25	1 RFID tag, 1 reader	23 (Fanta, Pepsi, Coke, vinegar, wood, plastic, ceramic, rubber, ...)	93.7%
RF-EATS [10] (2020)	Reflection	Dielectric permittivity	500-1000	1 RFID tag, 1 reader	16 (wine 2009, Wine 2012, alcohol, alcohol+methanol, perfume, ...)	85.8%
RF-ray [15] (2021)	Reflection	Dielectric permittivity	920.625-924.375	1 RFID reader, 7×7 tag array	Glass, wood, ceramic, cardboard, water, wine, Coke, oil, perfume	99.8%
Tamera [58] (2023)	Reflection	The reflection amplitude feature	920-926	1 RFID reader, 1 tag	Metal, plastic, paper, glass	96%
IntuWition [22] (2019)	Reflection	Polarization	2402-2482, 5030-5835	2 Wi-Fi devices	Copper, aluminum, human, plywood, birch	95%
In-baggage [23] (2021)	Reflection	Polarization	2402-2422	2 Wi-Fi devices	Fiber, metal, cotton, water in bags or boxes	97%
LiquID [26] (2018)	Penetration	Refractive index and loss factor	3744-4243.2	Wire-connected UWB Tx/Rx	33 liquids (Distilled water, mineral water, grape juice, apple juice, ...)	11.9% permittivity error
TagScan [16] (2017)	Penetration	RP-rate	920.625-924.375	1 RFID reader, 2 detached tags	16 (vinegar, coke, liquor, beer, apple, orange, chocolate, ...)	91%
WiMi [24] (2019)	Penetration	Phase and amplitude change measurements	5170-5330	2 Wi-Fi devices	Vinegar, honey, soy, milk, Pepsi, liquor, water, oil, Coke, sweet water	95%
LiqRay [27] (2022)	Penetration	Relative frequency response factor	1700-2600	1 USRP	Water, Sprite, Coke, Pepsi, black tea, green tea, peach juice, orange juice with 0/1/.../20% alcohol	94.9%

A. Misunderstanding of the Impact of Frequency

It is widely and implicitly utilized that the channel impulse response regarding the material is relevant to the frequency of the signal. Specifically, the majority of existing material identification works aggregate channel impulse responses at different frequencies, and their evaluation results show that a wider bandwidth containing a wider range of frequencies tends to support more precise identification.

However, they assume such relevancy to be invariant in the sensing model. In theory, the difference in the channel impulse response comes from the distinct reflection or penetration coefficient, and the coefficient is determined by the material's dielectric permittivity that varies with the frequency. Nevertheless, those works share an approximation that the dielectric permittivity remains constant across frequencies, which limits the precision of material identification. The dielectric permittivity can vary by over 10% [43] across the frequency range of 5-9 GHz or 77-81 GHz, making this approximation a nonnegligible source of precision loss.

To get rid of the coarse approximation, LiqRay [27] proposes a method to model the dielectric permittivity as a function of frequency, change the sensing goal into the permittivity-frequency curve and potentially diminish the loss.

B. Insufficient Validation of Material Features

It is likely to discover some features that distinguish a collection of objects through experiments. However, the majority of the features are invalid from the perspective of material identification because they distinguish objects mainly by their scale, shape and location instead of their material composition.

To validate a material feature, it is required to ensure that the material composition is the only major variable. In other

TABLE VI
COMMON EQUIPMENT AND SOFTWARE TOOLKITS FOR MATERIAL IDENTIFICATION.

Signal	Equipment	Software Toolkit	Model	Analysis	Feature
RFID	Impinj Reader R420	Octane SDK	Reflection	Frequency	RSS+phase
	USRP N210	GNU Radio Companion	Reflection	Time/Frequency	RSS+phase
	Any TX + Impinj RX	Octane SDK	Penetration	Frequency	RSS+phase
	Any TX + USRP RX	GNU Radio Companion	Penetration	Time/Frequency	RSS+phase
mmWave	TI IWR1642+DCA1000	mmWaveStudio	Both	Frequency	RSS+phase
	TI IWR6843+DCA1000	mmWaveStudio	Both	Frequency	2D RSS+phase heatmap
	Google Soli	Ripple	Reflection	Time/Frequency	RSS+phase
Wi-Fi	Intel WiFi Link 5300	PicoScenes	Reflection	Frequency	CSI
	Any TX + Intel WiFi Link 5300 RX	PicoScenes	Penetration	Frequency	CSI
UWB	Decawave Trek1000	DecaRangeRTLS ARM Source Code	Both	Frequency	RSS+phase

words, two conditions should be met: 1) the feature is consistent among objects with the same material composition yet different scales, shapes and locations; 2) the difference of the feature among objects with distinct material compositions is significantly larger than the measurement error of the feature.

To validate the first condition, raw reflected or penetrated signals of multiple objects under multiple settings are required. One recommended data source is open-source datasets that provide reliable data of various objects and settings. For example, the Wallabot material classification dataset [108] provides raw UWB signals (6.3-8.3 GHz) sampled at 100 GHz reflected from cement walls, ceramic floors, glass and 2 types of wood at different 3D positions relative to the transceiver. Another dataset RFVibe [74] provides raw mmWave signals (77-81 GHz) reflected from 23 objects made of cardboard, metal, glass, ceramic, plastic, foam and wood vibrating under the stimulation of different acoustic waves. If the signal or the materials in existing datasets do not satisfy the requirements, a custom dataset will be necessary. When recording the custom dataset, it is recommended to suppress interference from diffraction, diffuse reflection and multipath reflection by choosing large, smooth and thick objects.

To validate the second condition, accurate measurement of the indicator based on high-quality raw signal is critical. Commercial equipment and software toolkits are reliable and recommended for better accuracy. When choosing the equipment and software toolkit, it is required to consider the signal type, material identification model, analysis type and the utilized features in Table VI. For RFID developers, the Impinj Reader R420 [109] with the Octane SDK [110] can be applied. If the material identification method requires time-domain analysis, the Universal Software Radio Platform (USRP) series [111] with GNU Radio Companion [112] can be taken. For mmWave developers, commercial evaluation boards and data-capture adapters like TI IWR1642 [113] and DCA1000 [114] can be used with the mmWaveStudio software. When the spatial distribution of signal features is required (e.g. the object consists of multiple parts, or the object's location is unknown), the evaluation board can be replaced with TI IWR6843 [115]. If time-domain analysis is required, it is recommended to use Google's Soli radar with the Ripple [116] toolkit. For Wi-Fi developers, network interface cards like Intel WiFi Link 5300 [117] can be applied with a CSI-tool software like PicoScenes [5]. For UWB developers, evaluation kits like Decawave UWB Trek1000 [118] can be used with DecaRangeRTLS ARM Source Code [119].

C. Inappropriate Use of Classifiers

A classifier commonly takes the indicator of the material (e.g. CSI-based feature) as its input and outputs the material composition. A variety of classifiers have been proposed over the past decades, including the K-Nearest Neighbors (KNN) classifier, the Support Vector Machine (SVM), the Gradient Boosting Tree, the Multi-Layer Perceptron (MLP) and the Deep Neural Network (DNN). In recent years, deep learning based on DNNs has become a trend in material identification.

Nevertheless, it is not always appropriate to apply deep learning to material identification. First, the training process can be extremely costly. The architecture of a DNN can be greatly flexible and a large collection of hyperparameters needs to be optimized. Furthermore, for each collection of hyperparameters, the weights of the DNN are required to be optimized. As a result, both optimizations yield a high computational cost.

Moreover, deep learning can be more prone to interference if some feature extraction efforts are offloaded to learning. With the power of deep learning, it is possible to implement material identification with lower-level features that require less modeling effort. However, the deep neural network may identify materials through the spatial difference (e.g. the distance between the object and the transceiver) recorded in the dataset, which is undesired and hard to detect.

In most material identification tasks, the signal model contributes more than the classifier, and a lightweight machine learning model is recommended, including the KNN classifier and the Gradient Boosting Tree classifier. Those classifiers can be implemented with minimal effort using libraries like scikit-learn [120] and XGBoost [121], then trained with minimized time consumption. Moreover, if those models have poor performance, deep learning can be applied with minimal effort via toolkits like Keras [122].

VII. FUTURE DIRECTIONS

Despite the promising developments, there remain some open problems that impede the widespread application of material identification.

From the perspective of sensing, a wide range of objects in real life are not supported, including multi-layered objects (e.g. baggage [23], [123], bottled drink, the human body [104],

[124]), metallic objects, mixtures, thin or small objects and rough objects. Besides, the adaptability to complex environments is limited. Home and industrial environments involve material identification from a long range, in a non-line-of-sight (NLOS) scenario, or with multiple objects in the same space.

From the perspective of communication, it is potentially feasible to enhance communication by reconfiguring the environment according to the material composition information of objects, yet the model and algorithm for such enhancement/reconfiguration are unclear.

In this section, we will discuss some possible solutions to the open problems.

A. Extensions of the RF-based Material Identification Model

1) Identification of Multi-layered Material: The reflected or penetrated signal from a multi-layered object is the superposition of signals from each layer. In analyzing the superposition, two challenges occur: 1) the number of unknown variables increases as the dielectric permittivity and thickness of each layer are required to be solved; 2) different multi-layered materials may yield identical signal properties. Formally, let $a_1, a_2, ..., a_M$ denote an observed feature based on the RF-based model, $x_1, x_2, ..., x_N$ be the required variables and $F_1, F_2, ..., F_M$ be the RF-based model, then the equations $F_i(x_1, x_2, ..., x_N) = a_i (1 \leq i \leq M)$ can be underdetermined and the models F_i can be many-to-one.

To tackle the challenge, more equations are required. Equations can be established by tuning the parameters of existing models or building new models, and the variables can be determined when the number of equations is larger than or equal to the number of variables.

2) Quantitative Material Identification: Quantitative material identification refers to building a mathematical mapping between the RF signal properties and the material composition. Instead of collecting samples of all possible results as required in data-driven material classification [17], [22], human activity recognition [125] and so on, quantitative sensing investigates the physical mechanics of the interaction between the object and the RF signal. Therefore, it is possible to identify mixtures that have great significance to human health [126].

Quantitative material identification works in a two-phase way. In the first phase, the impact of the property (e.g. the mixture's dielectric permittivity) on the RF signal properties is modeled by electromagnetic rules; in the second phase, the property is translated to the concentration of each component with empirical formulas or lookup tables. For example, recent works on soil moisture sensing [21], [127], [128] measure the light of speed within the soil by the time of flight (ToF) of the RF signal, convert it to the dielectric permittivity with Eq. 7 and empirically translate the dielectric permittivity into the soil moisture.

The two-phase scheme in developing model-based methods can be promising as it offloads the link between material properties and material composition to third-party laboratories. Afterward, it is sufficient to develop a model-based material identification method only with a model connecting material properties and RF signal properties.

B. Novel Material Identification Models Based on Physical Principles

The scale and roughness constraints on the object come from the limitation of RF signals and the corresponding sensing model based on Snell's Law and Fresnel's Law. By innovating the sensing model with other physical principles [38], it is possible to break the constraints.

1) Polarimetry-based Model: Generated by common RF devices, the majority of RF signals are *linearly polarized* and can be decomposed into two orthogonal components, namely, the p-polarized and s-polarized one. According to Fresnel's Law, the impact of the reflection/penetration on the p-polarized and s-polarized components are different, which can be modeled and utilized for an indicator of materials.

The polarimetry-based sensing model can be utilized in various sensing applications [76], [129], including detection of metallic materials [22].

2) Diffuse-reflection-based Model: The assumption that the reflected signals are spectral limits the range of material identification. It requires the transceiver to face the object surface perpendicularly, taking the single-device setting as an example. When the object is far from the transceiver or the line of sight is blocked, the requirement can be unrealistic.

As no surfaces are absolutely smooth, there are reflected signals toward directions other than the spectral reflection direction. The Bidirectional Reflectance Distribution Function (BRDF) can model the reflected signal strength in each direction relative to the spectral-reflected signal strength. Furthermore, the BRDF can be instantiated as the Phong Model [130] when the object has a flat or convex surface, or the Lambert's Model [131] when the object has a roughness significantly larger than the wavelength of the signal.

Afterward, the long-range or NLOS material identification problem can be converted to a multi-variable sensing problem where the incident angle and the BRDF parameters are unknown, which can be solved by multi-variable sensing techniques.

3) Acoustic-based Model: Acoustic signals apply mechanical forces on objects and fetch a novel set of material properties that are inaccessible in RF-based sensing models, such as viscosity [132], surface tension [133] and resonant frequency [74], [134], [135].

The surface tension factor and viscosity are limited to liquids, while the polarization change and resonant frequency exist in both solid and liquid materials. Therefore, for all materials, the acoustic-based sensing model applies and may enable material identification in scenarios where RF signals cannot reach the object.

4) Visible-light-based Model: Looking into the microscope, visible light is compatible to extremely small objects, including a drop of human blood [6]. The RF-based techniques can also be migrated to visible light, as the diffraction loss [99] is negligible while the directionality [136], [137] and range resolution [138] are sufficient.

Moreover, some microscope physical effects can be observed by visible light, yielding novel models. First, the Brownian motion of speckles inside a drop of liquid can be detected with the range resolution of visible light. The

fluctuation of speckle intensity over time implies the viscosity of the liquid and the liquid's material composition. Second, visible light triggers photoacoustic effect [139]–[141] at the surface of the material. Specifically, the atoms can absorb the photons in visible light and transmit the light energy into mechanical energy. Afterward, by detecting the mechanical energy with a piezoelectric layer, small objects with different material compositions can produce different electric signals. Third, the molecules in dielectric materials can be resonant with terahertz signals, and the strength of resonance at certain frequencies indicates the concentration of certain molecules (e.g. water [8]).

C. RF Channel Reconfiguration Based on Material Identification

It is possible to improve certain communication channels in an indoor space by understanding the materials' impact on communication signals. Similar improvement has been achieved in the acoustic field that decorates a theatre with well-designed materials of certain composition and scale to optimize the sound effects in the audience area [142].

With the reflection and penetration model, the channel impulse response of each path can be calculated given the positions, scales and compositions of all materials within the path. Afterward, the superposed signal at the receiver can be modeled with the channel impulse responses. Furthermore, to enhance the superposed signal, a possible approach is to reconfigure some of the channel impulse responses by replacing materials. Physically trying and replacing materials can be exhaustive, yet reflective intelligent surfaces can reduce the complexity by emulating the reflection behaviors of common materials [143].

VIII. CONCLUSION

This paper provides a comprehensive survey of RF-based material identification methods. In the taxonomy, we categorize material identification models into the reflection-based and penetration-based ones. Methods with each model are further classified by the utilized signal type, including RFID, mmWave, Wi-Fi and UWB. For each branch, we illustrate the physical principle and present detailed descriptions of existing works. Afterward, we propose common evaluation metrics of material identification methods, including precision, accuracy, device deployment overhead and adaptability. According to the metrics, we then discuss the advantages and disadvantages of the reflection/penetration model and the four signal types. Moreover, we discuss common misconceptions and pitfalls for researchers, including misunderstanding of the impact of frequency, insufficient validation of material features and inappropriate use of classifiers. Furthermore, we explore future trends in material identification from the perspective of the sensing model and the signal. Material identification enables the connectivity of objects to the information domain and is deemed an extension of the current Internet of Things to be further explored in the coming years.

REFERENCES

[1] Y. Sun, W. Wang, L. Mottola, R. Wang, and Y. He, "Aim: Acoustic inertial measurement for indoor drone localization and tracking," in *Proceedings of ACM SenSys*, 2022, pp. 476–488.

[2] W. Wang, L. Mottola, Y. He, J. Li, Y. Sun, S. Li, H. Jing, and Y. Wang, "MicNest: Long-range instant acoustic localization of drones in precise landing," in *Proceedings of ACM SenSys*, 2022, pp. 504–517.

[3] J. Xie, H. Kong, J. Yu, Y. Chen, L. Kong, Y. Zhu, and F. Tang, "mm3DFace: Nonintrusive 3D facial reconstruction leveraging mmWave signals," in *Proceedings of ACM MobiSys*, 2023, p. 462–474.

[4] X. Xu, J. Yu, C. Ma, Y. Ren, H. Liu, Y. Zhu, Y.-C. Chen, and F. Tang, "mmECG: Monitoring human cardiac cycle in driving environments leveraging millimeter wave," in *Proceedings of IEEE INFOCOM*, 2022, p. 90–99.

[5] PicoScenes: Supercharging your next Wi-Fi sensing research! – PicoScenes documentation. [Online]. Available: https://ps.zpj.io/

[6] C. Liu, Y. Du, and L. Du, "A contactless glucose solution concentration measurement system based on improved high accurate FMCW radar algorithm," *Sensors*, vol. 22, no. 11, 2022.

[7] S. Yue and D. Katabi, "Liquid testing with your smartphone," in *Proceedings of ACM MobiSys*, 2019, p. 275–286.

[8] S. S. Afzal, A. Kludze, S. Karmakar, R. Chandra, and Y. Ghasempour, "AgriTera: Accurate non-invasive fruit ripeness sensing via sub-Terahertz wireless signals," in *Proceedings of ACM MobiCom*, 2023.

[9] U. Ha, Y. Ma, Z. Zhong, T.-M. Hsu, and F. Adib, "Learning food quality and safety from wireless stickers," in *Proceedings of ACM HotNets*, 2018, pp. 106–112.

[10] U. Ha, J. Leng, A. Khaddaj, and F. Adib, "Food and liquid sensing in practical environments using RFIDs," in *Proceedings of USENIX NSDI*, Feb. 2020, pp. 1083–1100.

[11] L. Zhong, M. Ouyang, F. Zhu, M. Jin, X. Wang, X. Guan, C. Zhou, and X. Tian, "SmartShell: A near-field reflective surface enhancing RSS," in *Proceedings of ACM MobiSys*. New York, NY, USA: Association for Computing Machinery, 2023, p. 124–136.

[12] C. Liaskos, G. Pyrialakos, A. Pitilakis, S. Abadal, A. Tsioliaridou, A. Tasolamprou, O. Tsilipakos, N. Kantartzis, S. Ioannidis, E. Alarcon, A. Cabellos, M. Kafesaki, A. Pitsillides, K. Kossifos, J. Georgiou, and I. F. Akyildiz, "ABSense: Sensing electromagnetic waves on metasurfaces via ambient compilation of full absorption," in *Proceedings of ACM NANOCOM*. New York, NY, USA: Association for Computing Machinery, 2019.

[13] B. Xie, J. Xiong, X. Chen, E. Chai, L. Li, Z. Tang, and D. Fang, "Tagtag: Material sensing with commodity RFID," in *Proceedings of ACM SenSys*, 2019, pp. 338–350.

[14] X. Lv, Y. Zhang, Q. Shi, M. Temiz, and A. El-Makadema, "Examining food quality via RFID tag array," in *Proceedings of IEEE ICMMT*, 2021, pp. 1–3.

[15] H. Ding, L. Zhai, C. Zhao, S. Hou, G. Wang, W. Xi, J. Zhao, and Y. Gong, "RF-ray: Joint RF and linguistics domain learning for object recognition," in *Proceedings of ACM IMWUT*, vol. 5, no. 3, 2021.

[16] J. Wang, J. Xiong, X. Chen, H. Jiang, R. K. Balan, and D. Fang, "Tagscan: Simultaneous target imaging and material identification with commodity RFID devices," in *Proceedings of ACM MobiCom*, 2017, pp. 288–300.

[17] H.-S. Yeo, G. Flamich, P. Schrempf, D. Harris-Birtill, and A. Quigley, "RadarCat: Radar categorization for input & interaction," in *Proceedings of ACM UIST*, 2016, pp. 833–841.

[18] C. Wu, F. Zhang, B. Wang, and K. J. R. Liu, "mSense: Towards mobile material sensing with a single millimeter-wave radio," in *Proceedings of ACM IMWUT*, vol. 4, no. 3, 2020.

[19] Y. Liang, A. Zhou, H. Zhang, X. Wen, and H. Ma, "FG-LiquID: A contact-less fine-grained liquid identifier by pushing the limits of millimeter-wave sensing," in *Proceedings of ACM IMWUT*, vol. 5, no. 3, 2021.

[20] D. Cao, Y. Lin, G. Ren, Y. Gao, and W. Dong, "mmLiquid: Liquid identification using mmWave," in *Wireless Sensor Networks*, H. Ma, X. Wang, L. Cheng, L. Cui, L. Liu, and A. Zeng, Eds., 2022, pp. 1–18.

[21] W. Chen, Y. Feng, M. Cardamis, C. Jiang, W. Song, O. Ghannoum, and W. Hu, "Soil moisture sensing with mmWave radar," in *Proceedings of ACM mmNets*, 2022, p. 19–24.

[22] D. Zhang, J. Wang, J. Jang, J. Zhang, and S. Kumar, "On the feasibility of Wi-Fi based material sensing," in *Proceedings of ACM MobiCom*, 2019.

[23] C. Shi, T. Zhao, Y. Xie, T. Zhang, Y. Wang, X. Guo, and Y. Chen, "Environment-independent in-baggage object identification using WiFi signals," in *Proceedings of IEEE MASS*, 2021, pp. 71–79.

[24] C. Feng, J. Xiong, L. Chang, J. Wang, X. Chen, D. Fang, and Z. Tang, "WiMi: Target material identification with commodity Wi-Fi devices," in *2019 IEEE ICDCS*, 2019, pp. 700–710.

[25] T. Zheng, Z. Chen, J. Luo, L. Ke, C. Zhao, and Y. Yang, "SiWa: See into walls via deep UWB radar," in *Proceedings of ACM MobiCom*, 2021, pp. 323–336.

[26] A. Dhekne, M. Gowda, Y. Zhao, H. Hassanieh, and R. R. Choudhury, "LiquID: A wireless liquid identifier," in *Proceedings of ACM MobiSys*, 2018, pp. 442–454.

[27] F. Shang, P. Yang, Y. Yan, and X.-Y. Li, "LiqRay: Non-invasive and fine-grained liquid recognition system," in *Proceedings of ACM MobiCom*, 2022, pp. 296–309.

[28] J. Xiao, Z. Zhou, Y. Yi, and L. M. Ni, "A survey on wireless indoor localization from the device perspective," *ACM Comput. Surv.*, vol. 49, no. 2, 2016.

[29] Z. Yang, C. Wu, Z. Zhou, X. Zhang, X. Wang, and Y. Liu, "Mobility increases localizability: A survey on wireless indoor localization using inertial sensors," *ACM Comput. Surv.*, vol. 47, no. 3, 2015.

[30] F. Gu, X. Hu, M. Ramezani, D. Acharya, K. Khoshelham, S. Valaee, and J. Shang, "Indoor localization improved by spatial context—a survey," *ACM Comput. Surv.*, vol. 52, no. 3, 2019.

[31] K. Ngamakeur, S. Yongchareon, J. Yu, and S. U. Rehman, "A survey on device-free indoor localization and tracking in the multi-resident environment," *ACM Comput. Surv.*, vol. 53, no. 4, 2020.

[32] C. Wan, L. Wang, and V. V. Phoha, "A survey on gait recognition," *ACM Comput. Surv.*, vol. 51, no. 5, 2018.

[33] F. Gu, M.-H. Chung, M. Chignell, S. Valaee, B. Zhou, and X. Liu, "A survey on deep learning for human activity recognition," *ACM Comput. Surv.*, vol. 54, no. 8, 2021.

[34] A. Uchiyama, S. Saruwatari, T. Maekawa, K. Ohara, and T. Higashino, "Context recognition by wireless sensing: A comprehensive survey," *Journal of Information Processing*, vol. 29, pp. 46–57, Jan 2021.

[35] D. Miyazaki, *Fresnel Equations*. Boston, MA: Springer, 2014, pp. 305–307.

[36] H. Jiang, J. Zhang, X. Guo, and Y. He, "Sense me on the ride: Accurate mobile sensing over a lora backscatter channel," in *Proceedings of ACM SenSys*, 2021, p. 125–137.

[37] X. Guo, L. Shangguan, Y. He, N. Jing, J. Zhang, H. Jiang, and Y. Liu, "Saiyan: Design and implementation of a low-power demodulator for LoRa backscatter systems," in *Proceedings of USENIX NSDI*, 2022, pp. 437–451.

[38] X. Guo, L. Tan, T. Chen, C. Gu, Y. Shu, S. He, Y. He, J. Chen, and L. Shangguan, "Exploring biomagnetism for inclusive vital sign monitoring: Modeling and implementation," in *Proceedings of ACM MobiCom*, 2024, pp. 93–107.

[39] D. M. Dobkin, *The RF in RFID: Passive UHF RFID in Practice*. Newnes, 2007.

[40] S. W. Smith, *The scientist and engineer's guide to digital signal processing*. USA: California Technical Publishing, 1997, ch. 9.

[41] H. E. Bennett and J. O. Porteus, "Relation between surface roughness and specular reflectance at normal incidence," *Journal of the Optical Society of America*, vol. 51, pp. 123–129, 1961.

[42] P. H. Fang, "Cole-Cole diagram and the distribution of relaxation times," *The Journal of Chemical Physics*, vol. 42, no. 10, pp. 3411–3413, 1965.

[43] A. Andryieuski, S. Kuznetsova, S. Zhukovsky, Y. Kivshar, and A. Lavrinenko, "Water: Promising opportunities for tunable all-dielectric electromagnetic metamaterials," *Scientific reports*, vol. 5, p. 13535, 08 2015.

[44] K. S. Cole and R. H. Cole, "Dispersion and Absorption in Dielectrics I. Alternating Current Characteristics," *The Journal of Chemical Physics*, vol. 9, no. 4, pp. 341–351, 2004.

[45] What is surface roughness?- unit, chart, measurement. [Online]. Available: https://www.engineeringchoice.com/what-is-surface-roughness/

[46] S. Pradhan, E. Chai, K. Sundaresan, L. Qiu, M. A. Khojastepour, and S. Rangarajan, "RIO: A pervasive RFID-based touch gesture interface," in *Proceedings of ACM MobiCom*, 2017, p. 261–274.

[47] Y. He, Y. Zheng, M. Jin, S. Yang, X. Zheng, and Y. Liu, "Red: Rfid-based eccentricity detection for high-speed rotating machinery," *IEEE Transactions on Mobile Computing*, vol. 20, no. 4, pp. 1590–1601, 2019.

[48] B. Braaten, G. Owen, and R. Nelson, *Design of Space-Filling Antennas for Passive UHF RFID Tags*, 2010.

[49] W. Stutzman and G. Thiele, *Antenna Theory and Design*. Wiley, 2012.

[50] J. SU and S. CHEN, "Dynamic sitting posture recognition system using passive rfid tags in internet of things," *Chinese Journal of Electronics*, vol. 33, no. 6, pp. 1–14, 2024.

[51] Z. Zhou, L. Shangguan, X. Zheng, L. Yang, and Y. Liu, "Design and implementation of an rfid-based customer shopping behavior mining system," *IEEE/ACM transactions on networking*, vol. 25, no. 4, pp. 2405–2418, 2017.

[52] L. K. Baxter, *Capacitive Sensors: Design and Applications*, 1997, pp. 6–36.

[53] M. Zhang, P. Li, S. Bao, and H. Xu, "RF-LqRNN: RFID-based concentration detection of alcohol solutions and glucose solutions," *IEEE Sensors Journal*, vol. 23, no. 10, pp. 10 656–10 672, 2023.

[54] J. Wang, L. Chang, S. Aggarwal, O. Abari, and S. Keshav, "Soil moisture sensing with commodity RFID systems," in *Proceedings of ACM MobiSys*, 2020, p. 273–285.

[55] C. Jiang, Y. He, X. Zheng, and Y. Liu, "Omnitrack: Orientation-aware rfid tracking with centimeter-level accuracy," *IEEE Transactions on Mobile Computing*, vol. 20, no. 2, pp. 634–646, 2021.

[56] E. Basar, M. Di Renzo, J. De Rosny, M. Debbah, M.-S. Alouini, and R. Zhang, "Wireless communications through reconfigurable intelligent surfaces," *IEEE Access*, vol. 7, pp. 116 753–116 773, 2019.

[57] W. Wang, Y. He, M. Jin, Y. Sun, and X. Guo, "Meta-speaker: Acoustic source projection by exploiting air nonlinearity," in *Proceedings of ACM MobiCom*, 2023.

[58] F. Shang, P. Yang, J. Xiong, Y. Feng, and X. Li, "Tamera: Contactless commodity tracking, material and shopping behavior recognition using COTS RFIDs," *ACM Transactions on Sensor Networks*, 2023.

[59] X. Liang, Y. Ma, C. Tian, W. Ning, B. Wang, and Y. Fu, "Dimar: A contactless material identification algorithm for complex permittivity of dielectrics via moving RFID system," *IEEE Transactions on Instrumentation and Measurement*, vol. 72, pp. 1–12, 2023.

[60] K. M. Bae, H. Moon, S.-M. Sohn, and S. M. Kim, "Hawkeye: Hectometer-range subcentimeter localization for large-scale mmWave backscatter," in *Proceedings of ACM MobiSys*, 2023, p. 303–316.

[61] C. Jiang, J. Guo, Y. He, M. Jin, S. Li, and Y. Liu, "mmVib: Micrometer-level vibration measurement with mmwave radar," in *Proceedings of ACM MobiCom*, 2020.

[62] J. Zhang, X. Na, R. Xi, Y. Sun, and Y. He, "mmHawkeye: Passive UAV detection with a COTS mmWave radar," in *Proceedings of IEEE SECON*, 2023.

[63] L. Xu, K. Wang, C. Gu, X. Guo, S. He, and J. Chen, "GesturePrint: Enabling user identification for mmWave-based gesture recognition systems," in *Proceedings of IEEE ICDCS*, 2024, pp. 1074–1085.

[64] C. X. Lu, S. Rosa, P. Zhao, B. Wang, C. Chen, J. A. Stankovic, N. Trigoni, and A. Markham, "See through smoke: Robust indoor mapping with low-cost mmWave radar," in *Proceedings of ACM MobiSys*. New York, NY, USA: Association for Computing Machinery, 2020, p. 14–27.

[65] K. Cui, Q. Yang, Y. Zheng, and J. Han, "mmRipple: Communicating with mmWave radars through smartphone vibration," in *Proceedings of ACM IPSN*, 2023, p. 149–162.

[66] J. Zhang, R. Xi, Y. He, Y. Sun, X. Guo, W. Wang, X. Na, Y. Liu, Z. Shi, and T. Gu, "A survey of mmWave-based human sensing: Technology, platforms and applications," *IEEE COMST*, 2023.

[67] Y. Huang and Y. Huang, "Challenges and opportunities of sub-6 ghz integrated sensing and communications for 5g-advanced and beyond," *Chinese Journal of Electronics*, vol. 33, no. 2, pp. 323–325, 2024.

[68] Y. Zhao, F. Zhou, L. Feng, W. Li, and P. Yu, "Madrl-based 3d deployment and user association of cooperative mmwave aerial base stations for capacity enhancement," *Chinese Journal of Electronics*, vol. 32, no. 2, pp. 283–294, 2023.

[69] The fundamentals of millimeter wave radar sensors. [Online]. Available: https://www.ti.com/lit/wp/spyy005a/spyy005a.pdf

[70] Y. Liu, S. Zhang, M. Gowda, and S. Nelakuditi, "Leveraging the properties of mmWave signals for 3D finger motion tracking for interactive IoT applications," *Proc. ACM Meas. Anal. Comput. Syst.*, vol. 6, no. 3, 2022.

[71] M. Gan, Y. Liu, L. Liu, C. Wu, Y. Dong, H. Zeng, and Z. Cao, "Poster: Mmleaf: Versatile leaf wetness detection via mmwave sensing," in *Proceedings of ACM MobiSys*, 2023, p. 563–564.

[72] J. Ahmadi-Shokouh, S. Noghanain, E. Hossain, M. Ostadrahimi, and J. Dietrich, "Reflection coefficient measurement for house flooring materials at 57-64 GHz," in *Proceedings of IEEE GLOBECOM*, 2009, p. 1247–1252.

[73] M. Gapeyenko, V. Petrov, D. Moltchanov, S. Andreev, Y. Koucheryavy, M. Valkama, M. R. Akdeniz, and N. Himayat, "An analytical represen-

tation of the 3GPP 3D channel model parameters for mmWave bands," in *Proceedings of ACM mmNets*, 2018, p. 33–38.
[74] H. Shanbhag, S. Madani, A. Isanaka, D. Nair, S. Gupta, and H. Hassanieh, "Contactless material identification with millimeter wave vibrometry," in *Proceedings of ACM MobiSys*. Association for Computing Machinery, 2023, p. 475–488.
[75] J. Wang, H. Jiang, J. Xiong, K. Jamieson, X. Chen, D. Fang, and B. Xie, "LiFS: Low human-effort, device-free localization with fine-grained subcarrier information," in *Proceedings of ACM MobiCom*, 2016.
[76] Y. Sun, Y. He, J. Zhang, X. Na, Y. Chen, W. Wang, and X. Guo, "BIFROST: Reinventing WiFi signals based on dispersion effect for accurate indoor localization," in *Proceedings of ACM SenSys*, 2023.
[77] X. Zheng, J. Wang, L. Shangguan, Z. Zhou, and Y. Liu, "Smokey: Ubiquitous smoking detection with commercial wifi infrastructures," in *IEEE INFOCOM 2016-The 35th Annual IEEE International Conference on Computer Communications*. IEEE, 2016, pp. 1–9.
[78] Y. Zeng, J. Liu, J. Xiong, Z. Liu, D. Wu, and D. Zhang, "Exploring multiple antennas for long-range WiFi sensing," in *Proceedings of ACM IMWUT*, 2022.
[79] Y. Zhang, Y. Zheng, K. Qian, G. Zhang, Y. Liu, C. Wu, and Z. Yang, "Widar3.0: Zero-effort cross-domain gesture recognition with Wi-Fi," *IEEE Transactions on Pattern Analysis and Machine Intelligence*, vol. 44, no. 11, pp. 8671–8688, 2022.
[80] D. Wu, Y. Zeng, R. Gao, S. Li, Y. Li, R. C. Shah, H. Lu, and D. Zhang, "WiTraj: Robust indoor motion tracking with WiFi signals," *IEEE Transactions on Mobile Computing*, vol. 22, no. 5, pp. 3062–3078, 2023.
[81] M. Xianjia, F. Lin, C. Hao, C. Ting, M. Jianfeng, W. Anwen, L. Dongdong, and Z. Yanfeng, "Just-in-time human gesture recognition using wifi signals," *Chinese Journal of Electronics*, vol. 30, no. 6, pp. 1111–1119, 2021.
[82] X. Zheng, K. Yang, J. Xiong, L. Liu, and H. Ma, "Pushing the limits of wifi sensing with low transmission rates," *IEEE Transactions on Mobile Computing*, pp. 1–15, 2024.
[83] L. Zhang, Y. Zhang, and X. Zheng, "Wisign: Ubiquitous american sign language recognition using commercial wi-fi devices," *ACM Transactions on Intelligent Systems and Technology (TIST)*, vol. 11, no. 3, pp. 1–24, 2020.
[84] A. V. Kityk, P. Huber, A. Andrushchak, P. Kula, and W. Piecek, "Application of retardation-modulation polarimetry in studies of nanocomposite materials," in *Proceedings of IEEE TCSET*, 2018, pp. 492–496.
[85] J. Singh and R. Banerjee, "A study on single and multi-layer perceptron neural network," in *Proceedings of IEEE ICCMC*, 2019, pp. 35–40.
[86] C. Xu, X. Zheng, Z. Ren, L. Liu, and H. Ma, "Uhead: Driver attention monitoring system using uwb radar," *Proceedings of the ACM on Interactive, Mobile, Wearable and Ubiquitous Technologies*, vol. 8, no. 1, pp. 1–28, 2024.
[87] Z. Luo, Q. Huang, R. Wang, H. Chen, X. Tao, G. Chen, and Q. Zhang, "WISE: Low-cost wide band spectrum sensing using UWB," in *Proceedings of ACM SenSys*, 2023, p. 651–666.
[88] Z. Chen, T. Zheng, C. Cai, and J. Luo, "MoVi-Fi: Motion-robust vital signs waveform recovery via deep interpreted RF sensing," in *Proceedings of ACM MobiCom*, 2021, p. 392–405.
[89] M. Zhao, T. Chang, A. Arun, R. Ayyalasomayajula, C. Zhang, and D. Bharadia, "ULoc: Low-power, scalable and cm-accurate UWB-tag localization and tracking for indoor applications," in *Proceedings of ACM IMWUT*, 2021.
[90] W. O'Reilly and R. Guza, "Comparison of spectral refraction and refraction-diffraction wave models," *Journal of Waterway Port Coastal and Ocean Engineering-asce*, vol. 117, 05 1991.
[91] I. Lindell and A. Sihvola, *Boundary Conditions in Electromagnetics*. John Wiley & Sons, Ltd, 2019, pp. 101–141.
[92] R. Feynman, R. Leighton, M. Sands, and E. Hafner, *The Feynman Lectures on Physics; Vol. I*. AAPT, 1965, vol. 33.
[93] J. A. Shaw, "Radiometry and the Friis transmission equation," *American Journal of Physics*, vol. 81, no. 1, pp. 33–37, 2013.
[94] Y. Chen, J. Guo, Y. Sun, H. Yao, Y. Liu, and Y. He, "Elase: Enabling real-time elastic sensing resource scheduling in 5g vran," in *Proceedings of IEEE/ACM IWQoS*, 2024.
[95] Y. He, W. Wang, L. Mottola, S. Li, Y. Sun, J. Li, H. Jing, T. Wang, and Y. Wang, "Acoustic localization system for precise drone landing," *IEEE Transactions on Mobile Computing*, vol. 23, no. 5, pp. 4126–4144, 2024.
[96] Y. He, J. Zhang, R. Xi, X. Na, Y. Sun, and B. Li, "Detection and identification of non-cooperative uav using a cots mmwave radar," *ACM Transactions on Sensor Networks*, vol. 20, no. 2, pp. 1–22, 2023.
[97] Y. Sun, W. Wang, L. Mottola, Z. Jia, R. Wang, and Y. He, "Indoor drone localization and tracking based on acoustic inertial measurement," *IEEE Transactions on Mobile Computing*, vol. 23, no. 6, pp. 7537–7551, 2024.
[98] W. Wang, Y. He, L. Mottola, S. Li, Y. Sun, J. Li, H. Jing, T. Wang, and Y. Wang, "Acoustic localization of drones in precise landing: The research and practice with micnest," *GetMobile: Mobile Computing and Communications*, vol. 27, no. 3, p. 27–32, 2023.
[99] F. Zhang, K. Niu, J. Xiong, B. Jin, T. Gu, Y. Jiang, and D. Zhang, "Towards a diffraction-based sensing approach on human activity recognition," in *Proceedings of ACM IMWUT*, 2019.
[100] W. Sun, I. Chansarkar, and K. Srinivasan, "Short: Liquid thickness sensing with backscattered signals for dysphagia," *Smart Health*, vol. 28, p. 100399, 2023.
[101] J. Liu, W. Li, T. Gu, R. Gao, B. Chen, F. Zhang, D. Wu, and D. Zhang, "Towards a dynamic fresnel zone model to wifi-based human activity recognition," in *Proceedings of ACM IMWUT*, 2023.
[102] X. Wang, K. Niu, A. Yu, J. Xiong, Z. Yao, J. Wang, W. Li, and D. Zhang, "WiMeasure: Millimeter-level object size measurement with commodity WiFi devices," in *Proceedings of ACM IMWUT*, 2023.
[103] L. Dodds, I. Perper, A. Eid, and F. Adib, "A handheld fine-grained RFID localization system with complex-controlled polarization," in *Proceedings of ACM MobiCom*, 2023.
[104] Z. Shi, T. Gu, Y. Zhang, and X. Zhang, "mmBP: Contact-free millimetre-wave radar based approach to blood pressure measurement," in *Proceedings of ACM SenSys*, 2023, p. 667–681.
[105] H. Hoang, "Near-field propagation analysis for traveling-wave antennas," in *Antenna Systems*. IntechOpen, 2021.
[106] What are near field and far field regions of an antenna? [Online]. Available: https://www.everythingrf.com/community/what-are-near-field-and-far-field-regions-of-an-antenna
[107] The fundamentals of millimeter wave radar sensors (rev. a). [Online]. Available: https://api.semanticscholar.org/CorpusID:234599194
[108] G. Agresti and S. Milani, "Material identification using RF sensors and convolutional neural networks," in *Proceedings of IEEE ICASSP*, 2019, pp. 3662–3666.
[109] Speedway reader documents & downloads. [Online]. Available: https://support.impinj.com/hc/en-us/articles/202755298-Speedway-Reader-Documents-Downloads
[110] Octane sdk - impinj support portal. [Online]. Available: https://support.impinj.com/hc/en-us/articles/202755268-Octane-SDK
[111] Ettus research - the leader in software defined radio (sdr) — ettus research, a national instruments brand — the leader in software defined radio (sdr). [Online]. Available: https://www.ettus.com/
[112] Sdr software - gnu radio - ettus research — ettus research, a national instruments brand — the leader in software defined radio (sdr). [Online]. Available: https://www.ettus.com/sdr-software/gnu-radio/
[113] IWR1642 data sheet, product information and support. [Online]. Available: https://www.ti.com/product/IWR1642
[114] DCA1000EVM evaluation board — ti.com. [Online]. Available: https://www.ti.com/tool/DCA1000EVM
[115] IWR6843 data sheet, product information and support. [Online]. Available: https://www.ti.com/product/IWR6843
[116] Ripple. [Online]. Available: https://www.cta.tech/Resources/Standards/Ripple#hub
[117] Support for intel wifi link 5300. [Online]. Available: https://www.intel.com/content/www/us/en/support/products/70971/wireless/legacy-intel-wireless-products/intel-wireless-series/intel-wifi-link-5300.html
[118] Trek1000 product brief datasheet by decawave limited. [Online]. Available: https://www.digikey.com/en/htmldatasheets/production/1727320/0/0/1/trek1000
[119] Trek1000 decawave development kit. [Online]. Available: https://www.decawave.com/sites/default/files/decawave_trek.exe
[120] scikit-learn: machine learning in python. [Online]. Available: https://scikit-learn.org/stable/index.html
[121] Xgboost documentation. [Online]. Available: https://xgboost.readthedocs.io/en/stable/
[122] Keras: Deep learning for humans. [Online]. Available: https://keras.io/
[123] Z. Li, Z. Yang, C. Song, C. Li, Z. Peng, and W. Xu, "E-Eye: Hidden electronics recognition through mmWave nonlinear effects," in *Proceedings of ACM SenSys*, 2018, p. 68–81.
[124] J. Sandby-Møller, T. Poulsen, and H. C. Wulf, "Epidermal thickness at different body sites: relationship to age, gender, pigmentation, blood content, skin type and smoking habits," *Acta dermato-venereologica*, vol. 83, no. 6, pp. 410–412, 2003.

[125] W. Jiang, C. Miao, F. Ma, S. Yao, Y. Wang, Y. Yuan, H. Xue, C. Song, X. Ma, D. Koutsonikolas, W. Xu, and L. Su, "Towards environment independent device free human activity recognition," in *Proceedings of ACM MobiCom*, 2018, p. 289–304.
[126] Alcohol and the human body. [Online]. Available: https://www.niaaa.nih.gov/alcohols-effects-health/alcohol-topics/alcohol-facts-and-statistics/alcohol-and-human-body
[127] U. M. Khan and M. Shahzad, "Estimating soil moisture using RF signals," in *Proceedings of ACM MobiCom*, 2022, pp. 242–254.
[128] Y. Feng, Y. Xie, D. Ganesan, and J. Xiong, "LTE-Based low-cost and low-power soil moisture sensing," in *Proceedings of ACM SenSys*, 2023, pp. 421–434.
[129] T. Li, D. Bai, T. Prioleau, N. Bui, T. Vu, and X. Zhou, "Noninvasive glucose monitoring using polarized light," in *Proceedings of the 18th Conference on Embedded Networked Sensor Systems*, 2020, p. 544–557.
[130] B. T. Phong, *Illumination for computer generated pictures*. New York, NY, USA: Association for Computing Machinery, 1998, p. 95–101. [Online]. Available: https://doi.org/10.1145/280811.280980
[131] S. J. Koppal, *Lambertian Reflectance*. Boston, MA: Springer US, 2014, pp. 441–443. [Online]. Available: https://doi.org/10.1007/978-0-387-31439-6_534
[132] Y. Huang, K. Chen, Y. Huang, L. Wang, and K. Wu, "Vi-Liquid: Unknown liquid identification with your smartphone vibration," in *Proceedings of ACM MobiCom*, 2021, pp. 174–187.
[133] X. Sun, W. Deng, X. Wei, D. Fang, B. Li, and X. Chen, "Akte-Liquid: Acoustic-based liquid identification with smartphones," *ACM Transactions on Sensor Networks*, vol. 19, no. 1, 2023.
[134] I. Borodina, B. Zaitsev, A. Teplykh, O. Karavaeva, G. Burygin, and O. Guliy, "Acoustic sensor for detection and identification of microbial cells directly in the liquid phase," in *Proceedings of IEEE IUS*, 2019, pp. 575–578.
[135] M. Khan, M. Q. Reza, and S. P. Sirdeshmukh, "A prototype model development for classification of material using acoustic resonance spectroscopy," in *Proceedings of IEEE IMPACT*, 2017, pp. 128–131.
[136] B. Coll-Perales, J. Gozalvez, and E. Egea-Lopez, "Adaptive beamwidth configuration for millimeter wave V2X scheduling," in *Proceedings of IEEE VNC*, 2021, pp. 83–86.
[137] X. Zhang, L. Chen, M. Feng, and T. Jiang, "Toward reliable non-line-of-sight localization using multipath reflections," in *Proceedings of ACM IMWUT*, 2022.
[138] S. Kruse, L. Serino, P. Folge, D. E. Oviedo, A. Bhattacharjee, M. Stefszky, J. C. Scheytt, B. Brecht, and C. Silberhorn, "A pulsed lidar system with ultimate quantum range accuracy," *IEEE Photonics Technology Letters*, vol. 35, no. 14, pp. 769–772, 2023.
[139] H. O. Durmuş, C. Birlikseven, B. Karaböce, and M. Seyitsoy, "Investigation of photoacoustic effect on different materials," in *Proceedings of IEEE TIPTEKNO*, 2022, pp. 1–4.
[140] T. W. Shen, T. K. Ou, and C.-C. Chang, "Histogram analysis of photoacoustic effect changes on different liquid samples," in *Proceedings of ACM ICMHI*, 2019, p. 17–20.
[141] T. Rahman, A. T. Adams, P. Schein, A. Jain, D. Erickson, and T. Choudhury, "Nutrilyzer: A mobile system for characterizing liquid food with photoacoustic effect," in *Proceedings of ACM SenSys*, 2016, pp. 123–136.
[142] M. Luykx, M. Vercammen, and R. Metkemeijer, "Acoustic design of theatres for natural speech and/or variable accoustics," in *Proceedings of the Institute of Acoustics*, vol. 34, 11 2009, pp. 24–31.
[143] S. Hassouna, M. A. Jamshed, M. Ur-Rehman, M. A. Imran, and Q. H. Abbasi, "Configuring reconfigurable intelligent surfaces using a practical codebook approach," *Scientific Reports*, vol. 13, 2023.

Yande Chen (Student Member, IEEE) received the B.E. degree in the School of Software from Tsinghua University in 2022. He is currently pursuing the Ph.D. degree with the School of Software, Tsinghua University. His research interests include Internet of things and wireless sensing.

Chongzhi Xu (Student Member, IEEE) received the B.E. degree from Qingdao University, China, in 2021. He is currently pursuing the Ph.D. degree with Beijing University of Posts and Telecommunications, China. His research interests include Internet of Things and wireless sensing.

Kexin Li (Student Member, IEEE) received the B.S. degree and the M.S. degree in the School of Electronic Information and Electrical Engineering, Shanghai Jiao Tong University in 2021 and 2024, respectively. She was supervised by Prof. Meng Jin. Her research interests include wireless sensing and RFID systems.

Jia Zhang (Student Member, IEEE) received the B.S. degree in the School of Software from Tsinghua University in 2019 and the PhD degree in the School of Software from Tsinghua University in 2024. His research interests include Internet of things and wireless sensing.

Xiuzhen Guo (Member, IEEE) is an assistant professor with the College of Control Science and Engineering, Zhejiang University. She received her B.E. degree from Southwest University, and her Ph.D. degree from Tsinghua University. Her research interests include wireless networks, Internet of Things, and mobile computing. She is a member of ACM.

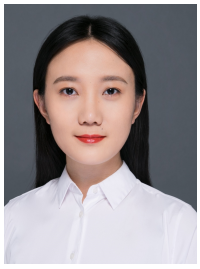

Meng Jin (Member, IEEE) is currently an associate professor at Shanghai Jiao Tong University. She is previously a post-doctoral researcher at School of Software and BNRist, Tsinghua University. She received the B.S., M.S. and Ph.d. degrees in Computer Science from Northwest University, Xi'an, China, in 2012, 2015, and 2018, respectively. Her main research interests include low-power wireless communication and wireless sensing.

Xiaolong Zheng (Member, IEEE) is currently an Associate Professor with the School of Computer Science, Beijing University of Posts and Telecommunications, China. He received his B.E. degree from the Dalian University of Technology, China, in 2011, and his Ph.D. degree from the Hong Kong University of Science and Technology, China, in 2015. His research interests include Internet of Things, wireless networks, and ubiquitous computing.

Yuan He (Senior Member, IEEE) received the B.E. degree from the University of Science and Technology of China, the M.E. degree from the Institute of Software, Chinese Academy of Sciences, and the Ph.D. degree from the Hong Kong University of Science and Technology. He is an Associate Professor with the School of Software and BNRist, Tsinghua University. His research interests include wireless networks, Internet of Things, pervasive, and mobile computing. He is a Senior Member of ACM.